Fluoride incorporation in high phosphate containing bioactive glasses and *in vitro* osteogenic, angiogenic and antibacterial effects

Jie Liu[a], Simon C.F. Rawlinson[a], Robert G. Hill[b], Farida Fortune[a*]

[a]Barts & The London School of Medicine and Dentistry, Institute of Dentistry, Queen Mary University of London, 4 Newark Street, London, E1 2AT, UK

[b]Unit of Dental Physical Sciences, Barts and The London, Queen Mary University of London, Mile End Road, London E1 4NS, UK

Abstract

Objectives: To manufacture and assess bioactivity of low fluoride/high phosphate (low F^-/high P_2O_5) bioglasses (BGs). Then the effects of BG-conditioned medium on osteoblast-like cell behaviour and BG particles on bactericidal activity were investigated.

Methods: BGs (0-7% F^- content, constant 6.33% P_2O_5 in mol %) were designed and produced. BG powder was immersed in Tris Buffer solution or α-MEM to determine apatite formation and ion (Ca, P, Si and F) release. Osteoblast-like cells MC3T3-E1 were treated with BG-conditioned medium and assessed for cytotoxicity, pre-osteogenic and pro-angiogenic responses. Antibacterial ability was explored by incubating sub-gingival bacteria with BG particulates.

Results: Rapid apatite formation was observed in F^- containing BGs after only 2-8 h immersion in Tris buffer solution. In the F^- free group, apatite was not detectable until 72 h. Peak Ca, P and F release into Tris buffer was at 2 h immersion, and then the levels decreased. In α-MEM, apatite formation in all the BGs was undetectable until 72 h immersion. Alkaline phosphatase activity, cell number, collagen formation, bone-like mineral nodules and osteogenic gene expression of MC3T3-E1 cells were significantly promoted in low F^- BG (P6.33F1) conditioned medium. MC3T3-E1 VEGF gene expression was increased, and protein production was dose-dependently promoted with F^- containing BG-conditioned medium. After incubation with BG particulates, the growth of sub-gingival bacteria, *A. actinomycetemcomitans* and *P. gingivalis,* was significantly inhibited; the antibacterial activity being dependent on the F^- content of the BGs.

Significance: These results show that low F^-/high P_2O_5 BGs significantly accelerated apatite formation and promoted both pre-osteogenic and pro-angiogenic responses

of MC3T3-E1 osteoblast-like cells and inhibited the growth of periodontal pathogens *in vitro*. These BGs may prove useful as bone graft substitutes.

Key words: bioactive glass, fluoride, phosphate, apatite, osteogenesis, angiogenesis, antibacterial

1. Introduction

Globally, the need for bone defect repair arises due to trauma, tumour, osteoporosis and other causes of skeletal tissue loss. In dentistry, periodontitis and peri-implantitis are common diseases associated with bone loss that require treatment. BG grafts, when exposed to body fluids, form a bone like apatite layer on their surface (a process termed 'bioactivity'), which is capable of forming a strong bond with the living bone. For this reason they are widely utilized in dental and orthopaedic applications [1].

Phosphate plays a vital role in BG bioactivity by forming a $CaO\text{-}P_2O_5$ rich bilayer: the new surface for apatite formation [2, 3]. ^{31}P and ^{29}Si magic-angle-spinning nuclear magnetic resonance (MAS-NMR) spectroscopy study demonstrates that phosphate is present largely as an orthophosphate phase in BGs results in an increase of the apatite deposition rate, which potentially promotes BG bioactivity [4, 5]. In the design of BGs, network connectivity (NC) is considered an important factor as it represents a measure of the number of bridging oxygen atoms per network forming element and an indicator of BG solubility, reactivity and ultimately bioactivity [6].

In fluoride containing BGs, fluoride complexes with calcium and sodium rather than forming Si-F bonds in BG structure, this results in a decrease in the compactness of the BG network [7-9]. Brauer *et al.* studied fluoride containing BGs by ^{19}F MAS–NMR and demonstrated the formation of fluorapatite (FAp, $Ca_{10}(PO_4)_6F_2$) [8], which is more acid resistant compared with hydroxyapatite (HA), has better stability and slow of degradation kinetics [10]. Numerous *in vitro* and animal studies have demonstrated that fluoride can regulate bone-forming cell activities and bone resorption [11-17], such as, affecting the RANKL/OPG system directly or indirectly [18], regulating BMP/Smads signalling pathway [12] or inhibiting NFATc1 gene expression to decrease osteoclastic activity [13]. Based on the characteristics of fluoride itself and the potential of forming FAp, local delivery of fluoride could reduce

demineralisation rate as well as enhancing re-mineralization to increase mineral density and clinically impact on the treatment strategies for osteoporosis [13, 19]. However, high levels of systemic fluoride are known to cause skeletal and dental fluorosis characterized by debilitating changes in the skeleton, and marked mottling and discoloration in the teeth [19, 20]. Nonetheless, the addition of fluoride into BGs and subsequent local delivery at beneficial concentrations would make such BGs more suitable than existing compounds for dental and orthopaedic problems.

Grafting can fail because of insufficient vascularisation deep within the body of the graft, thus angiogenesis and associated patent vascular network is crucial for optimal bone formation [21] and subsequent bone:graft contact, 'osseo-integration' [22]. Vascular endothelial growth factor (VEGF), released by osteoblastic and other cells, can promote differentiation of local mesenchymal stem cells into endothelial cells and subsequently activate the transmembrane VEFGR2 receptors in endothelial cells, which in turn activates several pathways responsible for angiogenesis [23-26]. This response would be expected to encourage bone formation secondary to increased vascularization throughout the graft substitute.

Another cause of graft failure is bacterial infections which hinder the repair of bone defects [27]. In particular, some oral pathogens associated with periodontal disease have also been associated with dental implant and defect repair failure [28]. Fluoride is widely incorporated into dental restorative materials, to encourage FAp formation, to reduce demineralisation and enhance re-mineralization, it also has anti-microbial properties [29]. Fluoride inhibits the dental plaque acid production that can result in demineralization [30, 31]. It acts directly as an enzyme inhibitor to interfere bacterial metabolism [32] and forms metal-fluoride complexes, most commonly AlF^{4-}, which interact with F-ATPase and nitrogenase enzymes resulting in inhibition of bacterial activity [33]. If fluoride released from BGs is available to influence local cell behaviour, then fluoride would be a useful constituent of BGs to reduce graft failure due to inappropriate vascularisation and infection.

We have created a series of BGs with high, constant phosphate content but with a varying and low fluoride addition, with a fixed BG NC. To determine whether such BGs maintained the characteristics that would make them suitable for potential use *in vivo,* the BGs bioactivity both in Tris buffer solution and cell culture medium were examined. Then, we further assessed the potential of BGs as modulators of

biological behaviour of osteoblast-like cells and bactericidal activity of the BG particles *in vitro*.

2. Materials and methods

2.1. BG synthesis

BGs in the system SiO_2-P_2O_5-CaO-Na_2O-CaF_2 (Table 1) were prepared by the melt-quench route. Briefly, mixtures of analytical grade SiO_2 (Prince Minerals Ltd., Stoke-on-Trent, UK), P_2O_5, Na_2CO_3, $CaCO_3$ and CaF_2 (Sigma-Aldrich Company Ltd., Gillingham, UK) were weighed in the appropriate amounts to give a batch size of 200 g. The batch was mixed thoroughly and placed in a platinum/rhodium crucible, and heated at 1360 ^{o}C for 60 min in an electrically heated furnace (Lenton EHF 17/3, Hope Valley, UK). After melting, the BGs were quenched rapidly into deionized water and the resulting frit was washed with ethanol then dried in a drying cabinet at 37 °C overnight. 100 g of each BG was ground in a Gyro mill (Glen Creston, London, UK) for two sets of 7 min and sieved by a mesh analytical sieve (Endecotts Ltd., London, UK) with a size of 38 µm to obtain fine powder. The amorphous structure of the BGs was tested using powder X-ray diffraction (XRD, PANalytical, Eindhoven, The Netherlands).

2.2. Ion release in Tris buffer

75 mg of each BG powder was dispersed in 50 mL Tris buffer solution, corresponding to a concentration of 1.5 g/L [34, 35]. All samples were placed in an orbital shaking incubator (KS 4000i Control, IKA, Staufen, Germany) at 37 °C with an agitation rate of 60 rpm for 2, 8, 24 and 72 hours.

For each time point, samples of each BG were removed from the incubator and the solutions were filtered with filter paper (4-13 µm pore retention, VWR International, Lutterworth, UK). The filtered solutions were next diluted 1:10 with deionized water and 1% nitric acid [34] and then analysed in an inductively coupled plasma–optical emission spectroscopy (ICP-OES; Varian Vista-PRO, Varian Ltd., Oxford, UK) to detect silicon, calcium, sodium, and phosphorus concentrations.

Fluoride-release into Tris buffer was measured using a fluoride-selective electrode (Orion 9609BNWP with Orion pH/ISE meter 710, both Thermo Scientific, Waltham, MA, USA).

2.3. Characterization of BG powders after immersion in Tris buffer

The filter papers collected from 2.2 were dried at 37 °C and the resultant powders were analysed using Fourier-transform infrared spectroscopy (FTIR; Spectrum GX, Perkin-Elmer, Waltham, MA, USA) data collected from 1800 to 500 cm^{-1} and XRD (PANalytical, Eindhoven, The Netherlands) data collected at room temperature with a 0.033° 2θ step size and a count rate of 99.6 s step-1, from 2θ values of 10° to 60°.

2.4. Cell culture and cytotoxicity of BG-conditioned medium

The mouse osteoblast-like cell line, MC3T3-E1, obtained from the Culture Collections (Public Health England, Porton Down, Salisbury, UK), was cultured under standard conditions (37 ºC, 5% CO_2/95% air, 100% humidity) in α-minimum essential medium (α-MEM, Lonza, London, UK) with 1% L- glutamine, 1% antibiotic (penicillin and streptomycin, Invitrogen, London, UK) and 5% foetal bovine serum (FBS, Lonza, London, UK).

75 mg BG particles from each group was immersed in 50 mL α-MEM with 1% antibiotic and kept shaking (60 rpm) for 2, 8, 24 and 72 h. For each time point, the samples were centrifuged (800 rpm, 5 min) to separate the solution and solid. The culture medium was then filtered with 0.2 μm pore size filters (VWR, Lutterworth, UK) for sterilization. Filtrate was further supplemented with sterile 1% L- glutamine and 5% FBS and used to treat MC3T3-E1 cells for 1, 3 and 5 days.

The cytotoxicity of BG-conditioned medium was quantified by MTT (3-[4, 5-dimethylthiazol-2-yl]-2, 5 diphenyl tetrazolium bromide) assay [36]. Briefly, medium was removed and cells were washed twice with PBS, then 30 μL 5 mg/mL tetrazolium salt MTT (Sigma-Aldrich Company Ltd., Gillingham, UK) was added to each well and incubated in 37 ºC for 4 h. Formazan crystals generated by mitochondrial enzyme activity were dissolved by dimethyl sulfoxide (DMSO, Sigma-Aldrich Company Ltd., Gillingham, UK) and the intensity of purple coloured reaction product quantified by measuring the absorbance spectra at 570 nm.

2.5. Ion release and apatite formation in cell culture medium

According to the cytotoxicity data, 72 h conditioned medium was chosen to detect concentrations of silicon, calcium, phosphorus, and fluoride in cell culture medium by ICP and fluoride-release was measured using a fluoride-selective electrode and the

dried powders were analysed using FTIR and XRD as previously performed on BG in Tris buffer.

2.6. Total quantification of cells cultured in BG-conditioned medium

BG-conditioned medium was used to identify the effect on cell proliferation by determining the DNA quantity in cultures using the fluorochrome, bisbenzimidazole (Hoechst 33258, Sigma-Aldrich Company Ltd., Gillingham, UK) [37, 38], in which increased fluorescence emission is linearly related to DNA concentration. MC3T3-E1 cells were cultured in 96-well plates in BG-conditioned medium for 7 d, 14 d and 21 d. On termination of the experiment, the cells washed in PBS, dried and lysed through a freezing and thawing cycle with 100 µL deionized water in each well to rupture cells and release DNA. The resulting lysate was then reacted with fluorochrome bisbenzimidazole (1:50) in TNE buffer with 10 mM Tris, 1 mM EDTA and 2 M NaCl (pH 7.4, Sigma-Aldrich Company Ltd., Gillingham, UK) and the resultant fluorescence intensity was measured at 460 nm emission and 355 nm excitation. Accurate cell number was determined by comparing fluorescence intensity with an established standard curve, which is a linear correction between fluorescence intensity and the cell number over a broad range (Fig. S1).

2.7. Alkaline phosphatase (ALP) activity in cells cultured in BG-conditioned medium

Cells were treated as for the cell proliferation experiments. ALP activity was measured by an enzyme histochemical assay [39, 40], in which ALP converts ρ-nitrophenyl phosphate to ρ-nitrophenyl. At each time point, cells were lysed through a freezing and thawing process and reacted with a solution of 2.5 mg/mL 4-nitropheyl phosphate disodium salt hexahydrate in Tris buffer solution with 1 mM $MgCl_2$ (pH = 9.5, Sigma-Aldrich Company Ltd., Gillingham, UK) for 40 min in 37 ^{o}C. 0.5 M NaOH was used to stop the reaction and the intensity of yellow colour reaction product was quantified by measuring the absorbance at 405 nm. ALP activity of the test samples were calculated and expressed as nmol/mL/min from calibration curve [41].

2.8. Detection and quantification of collagen formation in BG-conditioned medium

BG-conditioned medium was further supplemented with 5 mM β-glycerophosphate and 50 µg/mL L-ascorbic acid (Sigma-Aldrich Company Ltd., Gillingham, UK) to prepare osteogenic medium.

Collagen formation was quantified by measuring the concentration of Sirius red stain incorporated in cell-mediated matrix formation [42, 43]. MC3T3-E1 cells were treated for 2, 3 and 4 weeks with BG-conditioned osteogenic medium. Post incubation, cells were fixed for 10min in 2.5% glutaraldehyde at 4ºC and washed three times in deionized water. Cells were next incubated in 0.1% Sirius red F3B in a 1.3% saturated aqueous solution of picric acid (Sigma-Aldrich Company Ltd., Gillingham, UK) for 1 h at room temperature. Cultures were then washed twice with 0.5% acidified water and three times in deionized water to remove the unincorporated dye. Stained cultures were photographed followed by a dye extraction procedure using a mixture of 0.1 M NaOH and absolute methanol (1:1, Sigma-Aldrich Company Ltd., Gillingham, UK) for 30 min at room temperature. 200 µL aliquots of eluted dye were transferred to a 96-well plate and measured the absorbance at 570 nm.

2.9. Detection and quantification of mineralization in BG-conditioned medium

For the detection of bone nodule formation, at each time point, osteogenic medium was removed and cells were washed twice with PBS and fixed in 2.5% glutaraldehyde at 4 ºC for 10 min. After deionized water washing 200 µL of 40 mM Alizarin Red S (pH 4.1, Sigma-Aldrich Company Ltd., Gillingham, UK) was added per well. The plates were incubated at room temperature for 40 min and washed three times with deionized water to remove unincorporated dye.

For quantification of staining, an adaptation of the protocol described by Stanford et al. [44] was followed. Alizarin Red S was extracted from the monolayer by incubation in 10% (w/v) cetylpyridinium chloride (CPC, Sigma-Aldrich Company Ltd., Gillingham, UK) in 10 mM sodium phosphate, pH 7.0, for 30 min at room temperature. The dye was then removed and 100 µL aliquots transferred to a 96-well plate prior to absorbance reading at 570 nm.

2.10. Osteogenic gene expression in BG-conditioned medium by quantitative Reverse Transcription polymerase chain reaction (qPCR)

After treatment in BG-conditioned medium for 1, 4, 7, 14 and 21 d, total RNA of MC3T3-E1 was isolated using RNeasy mini kit (Qiagen, Manchester, UK) according

to the manufacture's protocol. RNase-Free DNase set (Qiagen, Manchester, UK) was used to eliminate DNA contamination in RNA samples. The purity of the isolated RNA was determined by measuring the optical density (OD) value (*A260/A280*) using the NanoDrop™ 1000 Spectrophotometer (Thermo Scientific, UK). cDNA synthesis was performed using the transcriptor first strand cDNA synthesis kit (Roche, UK) at 42 ºC for 30 min, 85 ºC for 5 min, 4 ºC for 5 min and the products were stored in -20 ºC. Quantitative RT-PCRs were carried out using the DNA Master SYBR Green I Kit (Roche Diagnostics, England, UK) in the 96-well LightCycler 480 qPCR system (Roche, UK) according to the manufacturer's instructions. Glyceraldehyde-3-phosphate dehydrogenase (GAPDH) was used as a housekeeping gene. The relative gene expression level was determined by comparing against the reference gene and normalised by the control group (normal medium treatment). All primers used in this study are listed in Table 2.

2.11. Angiogenesis gene expression and protein production in BG-conditioned medium by qPCR and Western blot

The VEGF gene expression was performed as previously described and the primers used are listed in Table 2.

To ascertain VEGF protein production, after treatment for the indicated periods, all the cells were washed twice with cold PBS and then lysed, homogenized and sonicated in RIPA lysis buffer containing 150 mM NaCl, 1.0% NP-40, 0.5% sodium deoxycholate, 0.1% sodium dodecyl sulphate (SDS), 50 mM Tris-HCl, pH 8.0 and freshly added Protease Inhibitors (Roche, UK). Lysates were centrifuged at 16,000×g for 20 min in 4 ºC. The protein concentration was determined by *DC* protein assay (Bio-Rad, UK). 4x LaemmLi sample buffer (Bio-Rad, UK) was added to the lysates followed with boiling at 100 ºC for 5 min and storage at -20 ºC. Aliquots of the denatured proteins were separated by 10% NuPAGE® Bis-Tris gel (Thermo scientific, UK), transferred electrophoretically to polyvinyl difluoride (PVDF) membrane (Thermo scientific, UK) and soaked in a blocking buffer (5% non-fat milk in TBST buffer containing 20 mM Tris–HCl, pH 7.5, 0.5 M NaCl, 0.1% Tween 20) for 1 h at room temperature. Subsequently, the membrane was incubated in blocking buffer with primary antibodies overnight at 4 ºC followed by three times TBST wash and secondary antibody incubation at room temperature for 1 h. Detection of protein antibody complex was performed by the ECL Western blot detection system

(Thermo scientific, UK). Cyclophilin B was used as a loading control. The following antibodies were used in this study: anti-VEGF antibody (1:2000, Abcam, UK), anti-Cyclophilin B antibody (1:6000, Abcam, UK) and Goat anti-Rabbit IgG (H+L) Secondary Antibody (1:2000, Thermo scientific, UK).

2.12. Antibacterial studies

Typical sub-gingival bacteria, *Aggregatibacter actinomycetemcomitans* and *Porphyromonas gingivalis* (kindly gifted by Professor Rob Allaker, Queen Mary University of London), were grown in brain heart infusion agar plates (Fisher Scientific, Loughborough, UK) for 48 h at 37 °C under anaerobic conditions. Then the log phase cultures were harvested and the bacterial concentrations were measured by reading absorbance at 595 nm.

BG particulates were sterilized by autoclaving (dry cycle) at 121 °C for 15 min and added to brain heart infusion broth at concentrations of 1.25, 2.5, 5, 10 and 20 mg/mL and plated in 96-well plates (100 µL/well). The bacteria (10^6 to 10^7 CFU/mL) were added subsequently (100 µL/well). Therefore, the final BG particle working concentrations were 0.625, 1.25, 2.5, 5 and 10 mg/mL. Sodium Fluoride (NaF) concentrations (2, 1, 0.5, 0.25, 0.125 and 0 mM) in brain heart infusion broth were used to treat bacteria as well to investigate the antibacterial effects of F^-. After incubation under anaerobic conditions for 0, 2, 4 and 8 h, 20 µL alamarBlue (Bio-Rad, UK) was added to each well and incubated for 1h according to the manufacture's protocol. Then the plates were centrifuged for 10 min at 4000 rpm and 100 µL aliquots transferred to new black 96-well plates to measure fluorescent intensity at 590 nm emission and 560 nm excitation. Percent inhibition of bacterial growth was then defined as 1 - (mean fluorescence of test wells / mean fluorescence of negative control well) × 100% following the manufacturer's instructions [45, 46].

2.13. Statistical analysis

The elemental analysis was carried out with three samples per group. Cell assay data with BG-conditioned medium are presented as means ± standard errors and represent data from six replicates per experiment. qPCR and Western blot assay were performed with three samples per group and bacterial studies were four replicates. Comparisons of cell assay data were made using a one-way analysis of variance (ANOVA). Significance is indicated when $P \leq 0.05$.

3. Results

3.1. BG formation

XRD patterns show that all the prepared BGs exhibited broad halos, which is the typical feature of an amorphous structure (Fig. 1). Therefore, we can confirm that these BGs with high phosphate and low fluoride additions still retained the appropriate non-crystalline structure.

3.2. Apatite formation in Tris buffer

Fluoride added to BG compositions causes significant changes in the XRD traces and FTIR spectra after immersion in Tris buffer solution for 8 h, compared with the fluoride free glass (Fig. 2 and Fig. 3).

In the XRD traces, patterns of hydroxyapatite (JCPDS 09-432), fluorapatite (15-876), carbonated hydroxyapatite (JCPD 19-272) and carbonated fluorapatite (JCPDS 31-267) all overlap [8]. Therefore, the term of 'apatite' in the XRD traces is referred to here to cover these species.

After 8 h immersion in Tris buffer solution, the typical apatite peaks at 26º, 32–34º, 47º, 50º and 52º 2θº (JCPDS 9-432) appear in traces for the fluoride containing BGs. These peaks become intense and more clearly pronounced as fluoride content increased from 1 mol% to 7 mol%. For the BG P6.33F0, the XRD pattern shows a small peak at around 28.5º 2θ (starred), which may indicate the presence of a small amount of calcite ($CaCO_3$).

After immersion in Tris buffer solution for 8 h, the FTIR spectra shows the sharpening of the Si-O-Si stretch band at about 1030 cm^{-1} in fluoride added BGs P6.33F1 to P6.33F7 (Fig. 3). At the same time, new bands appeared at around 800 cm^{-1}, which were assigned to Si-O-Si bond vibration between two adjacent SiO_4 tetrahedra as described previously for SBF-treated BGs [8]. These changes indicate the formation of a silica-gel surface layer after leaching of Ca^{2+} and Na^{+} ions and formation of Si-OH groups in these ion-depleted BGs.

A single band, or a split band at approximately 560-600 cm^{-1}, is the most characteristic region for apatite and other orthophosphates. After immersion in Tris buffer for 8 h, a single band in this region appeared in the high phosphate but fluoride free BG P6.33F0 and suggests the presence of a disordered apatite or

amorphous calcium phosphate. Characteristic split bands at 560 and 600 cm^{-1} appeared in the fluoride containing BGs P6.33F1 to P6.33F7 and suggest that adding fluoride significantly accelerates apatite formation.

Bands at about 870 cm^{-1} in the fluoride containing BGs after immersion in Tris buffer for 8 h indicate the presence of carbonate substitution in the apatite. It is noted that this carbonate band is an indicator of carbonate incorporated into the apatite, resulting in the formation of hydroxycarbonate apatite, rather than stoichiometric HAp [47]. Furthermore, broad CO_3^{2-} bands are present in the region starting from 1410 cm^{-1} indicating a B-type substitution (i.e. carbonate replacing a phosphate group), rather than an A-type substitution (i.e. carbonate replacing a hydroxyl group), which would be shifted to higher wave numbers, starting from 1460 cm^{-1} [8].

After immersion in Tris buffer, the XRD traces and FTIR spectra of BG P6.33F1 (CaF_2=1 mol%) showed significant changes compared with the pattern and spectrum of the unreacted glass (0 h) (Fig. 4 and Fig. 5). Within 2 h exposure to the Tris buffer solution, a small apatite peak at 26º 2θº appeared in the XRD trace. As immersion time increased, these typical apatite peaks at 26º and 32–34º 2θº become larger in intensity and more clearly pronounced. These data are consistent with the readings from the FTIR spectra: disappearance of the NBO (non-bridging oxygens, $Si–O^-$ $alkali^+$) band at 920 cm^{-1}, sharpening of the Si–O–Si stretch band at about 1030 cm^{-1}, new bands appeared at about 800 cm^{-1} and a single band at 560-600 cm^{-1} indicates the presence of non-apatite or amorphous calcium phosphate was observed after 2 h immersion. As immersion time increased to 8 h, the characteristic split band at 560 and 600 cm^{-1} appeared indicative of calcium phosphate crystallites.

3.3. Ion release in Tris buffer

The Ca and P concentrations in Tirs buffer reached a maximum after 2 h immersion and then dropped drastically from 2 h to 8 h (Fig. 6A, C), which is consistent with the results of XRD and FTIR: apatite formed in the fluoride containing BGs after 2 h to 8 h immersion.

Compared with the fluoride containing BGs, the P concentration in solution of P6.33F0 was much higher after 8 h immersion (Fig. 6C), which indicates that the incorporation of fluoride into these glasses promotes phosphate consumption and accelerates apatite formation.

P6.33F1, the lowest fluoride containing BG in this study, shows some amorphous calcium phosphate formation in the XRD and FTIR patterns after 8 h exposure in Tris buffer. It explains the reason for P concentration from P6.33F1 being slightly higher than those in the other higher fluoride content BGs at the time point of 8 h (Fig. 6C).

The fluoride concentrations in Tris buffer solution increased significantly after 2 h immersion in all the investigated BGs (Fig. 6E). In the low fluoride containing BGs, P6.33F1 and P6.33F3, F concentrations decreased gradually from 2 h to 72 h. However, when glass fluoride content increased from 5 mole % to 7 mole %, the solution fluoride was relatively constant.

Silicon and sodium concentrations increased sharply in the first 2 h immersion and then remained relative constant in the remaining experimental time (Fig. 6G, H).

3.4. Cytotoxicity of BG-conditioned medium

Compared with the control (normal medium without glass immersion), all the BG-conditioned medium samples, except 7% F^- glass at 72 h, were not cytotoxic to the growth of MC3T3-E1 cells (Fig. 7 A, B, C, D). In the 72 h conditioned medium, levels of MTT reaction products were significantly higher in the BG groups, 0-3% F content. However, this increase is small, and might be without meaning.

3.5. Ion release in cell culture medium

After 72 h immersion in α-MEM, solution calcium concentrations increased slightly as BGs fluoride content increased from 0% to 7% (Fig. 8). In the fluoride free and low fluoride containing BGs (P6.33F0, P6.33F1 and P6.33F3), solution calcium concentrations dropped slightly in comparison with that in the α-MEM. However, for the high fluoride containing BG, P6.33F7, calcium concentrations were significantly higher than that in α-MEM.

Phosphate concentration in all the BG compositions was constant, however, the released concentrations in all the groups were little lower than that in the α-MEM and dropped gradually as the BG fluoride content increased from 0% to 5%.

As supplied, α-MEM is silicon and fluoride free, F concentrations in the medium increased gradually as the BG fluoride content increased from 0% to 7% during 72 h immersion. Silicon concentrations in the α-MEM was the greatest in the P6.33F0

group and dropped slightly as the BG fluoride content increased, which is consistent with the BG composition (Table 1).

3.6. Apatite formation in cell culture medium

After 72 h immersion in α-MEM, there were subtle differences between the untreated and treated BGs in the XRD traces (Fig. 9). All the treated BGs showed similar patterns and with no obvious apatite diffraction line. A small peak at around 28.5º 2θ appeared in glass P6.33F5, which may indicate the presence of a small amount of calcite ($CaCO_3$) instead of apatite.

In the FTIR spectra, compared with the untreated BG with a non-bridging oxygen band at 920 cm^{-1}, all the treated BGs showed the disappearance of 920 cm^{-1} band and the sharpening of the Si-O-Si stretch band at about 1030 cm^{-1} (Fig. 10). It indicates the formation of a silica-gel surface layer after leaching of Ca^{2+} and Na^{+} ions and the formation of Si-OH groups. In all the treated BGs, a single P-O band was observed at around 570 cm^{-1} suggesting an amorphous or disordered crystalline apatite formation [48, 49]. Furthermore, in the F containing BGs, new bands at about 870 cm^{-1} and further broad bands starting from 1410 cm^{-1} indicate possible carbonate replacement of phosphate in the formed apatite.

3.7. Total quantification of cells cultured in BG-conditioned medium

MC3T3-E1 proliferation in 72 h conditioned medium varied depending on the BG composition (Fig. 11). The number of cells that survived was too few to be detected in the high F addition group (P6.33F7), and cell number was significantly lower in the P6.33F5 group compared with the control group. However, significantly more cells were observed in P6.33F0 and P6.33F1 groups than non-conditioned medium (control) from 7 d to 21 d in culture.

3.8. Alkaline phosphatase (ALP) activity in cells cultured in BG-conditioned medium

After treatment for 7 d, 14 d and 21 d in the BG-conditioned medium, MC3T3-E1 cells in the P6.33F0 and P6.33F1 groups demonstrated significantly higher ALP activity than those of the control. At time points 14 d and 21 d, ALP activity in P6.33F1 was significantly higher than that in P6.33F0, while in the 5% F addition glass (P6.33F5), ALP activity was significantly supressed (Fig. 12).

3.9. Collagen formation in BG-conditioned medium

Collagen formation was significantly promoted in P6.33F0 and P6.33F1 groups in comparison with that in control after 2 w, 3 w and 4 w culture (Fig. 13). At the time points of 2 w and 3 w, P6.33F1 conditioned medium induced more collagen formation than P6.33F0. However, in the latest time point (4 w); it was significantly supressed in 5% F addition group (P6.33F5).

3.10. Cell mineralization in BG-conditioned medium

MC3T3-E1 mediated mineralization in BG-conditioned medium was significantly promoted in the P6.33F0 and P6.33F1 groups, in comparison with the control after 2 w, 3 w and 4 w cultures (Fig. 14). At 2 w and 3 w, mineralization in P6.33F1 was significantly higher than that in P6.33F0. For the P6.33F3 group, mineralization was significantly promoted in the later time points (3 w and 4 w). However, in the 5% F addition group (P6.33F5), mineralization was significantly supressed in all the treatment periods.

3.11. Osteogenic gene expression in BG-conditioned medium

The expression of genes associated with osteogenesis, Col1a1 and OPN, are shown in Fig. 15. Both gene expressions were increased in the P6.33F0 and P6.33F1 groups in comparison to those in the control from 1 d to 21 d. Furthermore, they were greater in P6.33F1 than those in the P6.33F0 through the whole experimental period. Both Col1a1 and OPN gene expressions were significantly decreased in the P6.33F5 group.

3.12. Angiogenic gene expression and protein production in BG-conditioned medium

Compared with the control, VEGF gene expression was promoted by all the investigated BGs (P6.33F0 to P6.33F5) from 1 d to 21 d treatment (Fig. 16). When comparing the fluoride free glass (P6.33F0) with fluoride containing BGs (P6.33F1 to P6.33F5), the presence of fluoride further promoted VEGF gene expression.

VEGF protein production (Fig. 17), however, was not significantly different between BG and control groups at 7 d. In the 14 d and 21 d samples, greater VEGF protein production was observed in all the BG groups. Similar to VEGF gene expression, the

protein expression was also further promoted by the fluoride containing BGs compared with the fluoride free BG (P6.33F0).

3.13. Antibacterial studies

The antibacterial activity on *P. gingivalis* was significantly dependent on the BG particulate concentrations after 4 h incubation (Fig. 18). For the *A. actinomycetemcomitans,* however, P6.33F0 showed very low bactericidal activity and no change was observed as the particle concentration varied. When BG F content increased to 1-3%, antibacterial activity on *A. actinomycetemcomitans* significantly rose and was dependent on the particle concentrations. However, the particle concentration dependent effects decreased as the BG F content increased to 5 and 7%.

With 1.25 mg and 10 mg BG particulate treatment (Fig. 19), the antimicrobial activity on *A. actinomycetemcomitans* increased drastically as BG F content increased after 2h to 8h incubation.

For the *P. gingivalis*, with 1.25 mg BG particle treatment, the antibacterial activity increased significantly as the BG F content increased. However, when incubation time extended from 2 h to 8 h, the killing effects in low F BGs, 0-3% F, dropped when the particle concentration increased to 10 mg, the antibacterial activity increased significantly and there was no difference between BGs after 2 h and 4 h incubation. However, when extended to 8 h, the killing effects dropped drastically in the 0-1% F BGs.

To determine whether this was due solely as a function of F in the BGs, the effects of NaF concentrations on the viability of *P. gingivalis* and *A. actinomycetemcomitans* were carried out. Both bacteria were found to be sensitive to the F concentrations (Fig. 20). However, the antimicrobial activity of NaF on *A. actinomycetemcomitans* was significantly higher than that on the *P. gingivalis.*

4. Discussion

It is believed that increasing the P_2O_5 content in BGs enhances the reactivity as the phosphate is regarded to exist as a separate phase within the glass which is considerably more soluble than the silicate phase, resulted in faster apatite formation

[3-5]. However, we found that the formation of apatite occurred even more rapidly with the addition of fluoride (as low as only 1 mol %). Numerous experimental studies have reported that octacalcium phosphate (OCP) is a precursor phase involved in apatite formation *in vitro* [50-55]. Eanes *et al.* demonstrated that the presence of fluoride eliminated the formation of the intermediate OCP phase [56], and yet only 0.1–2 mg/L fluoride in the mineralization solution would promote the hydrolysis of OCP to apatite [57, 58]. In addition, as little as 1 mg/L fluoride was found to promote formation of needle-like nano-crystals, which are similar to native crystals in width and thickness and therefore have the potential to possess similar mechanical properties [58, 59].

Although the phosphate content was kept constant in all the BGs, the released P concentrations were variable, and as a function of the BG fluoride content. From 8 h to 72 h immersion in Tris buffer, the solution P concentration dropped sharply between the P6.33F0 and P6.33F1 (Fig. 6D). This further indicates that the combination of high phosphate content with a small amount fluoride significantly promotes the apatite formation rate evidenced through the consumption of phosphate from solution.

Compared to Tris buffer solution testing, experiments with cell culture medium provide a more *in vivo-like* model to examine how bodily fluids will interact with BGs. After 72 h immersion in α-MEM we observed a single band at approximately 570 cm^{-1} in FTIR spectra, corresponding to the formation of an amorphous or disordered crystalline apatite such as amorphous calcium phosphate, which is considered as a precursor of apatite. O'Donnell *et al*. found that apatite formed in physiological solution SBF was in nano-sized crystals [3], which would result Scherrer line broadening of the apatite peaks in XRD. Compared with the apatite formation in Tris buffer, it is much slower in α-MEM. Sepulveda *et al.* attributed the delayed surface apatite formation in cell culture media to the presence of proteins from serum [60]. In this study, however, serum was not added until the BG-conditioned α-MEM was used to treat cells. Magnesium (Mg) is involved in protein and nucleic acid synthesis, cell cycle, cytoskeletal integrity and bone remodelling [61] and is included in cell culture medium (α-MEM) at a concentration of 0.8 mM. Numerous studies have demonstrated that Mg^{2+} ion retards apatite formation by adsorption onto crystal surfaces and blocking active growth sites, irrespective of whether Mg^{2+} ion originates

from test medium or from the BG [62-64]. Although Mg^{2+} slows down apatite layer formation, it is found to increase the layer thickness [63, 65]. In addition, these *in vitro* Tris buffer and cell culture medium studies differ from the BG dissolution mechanism and kinetics *in vivo*. The continuous flow of physiological fluids can promote continuous BG dissolution, leading to thicker apatite layers *in vivo* [60].

Our cell culture experiments demonstrated clear effects of BG composition on the proliferation, ALP activity, collagen and bone nodule formation, osteogenic gene expression, VEGF gene expression and protein production of osteoblast-like cells (MC3T3-E1). Cytotoxicity is not evident in the high phosphate and F free or low F BGs (P6.33F0 to P6.33F3) but significantly suppressed growth rate when the F content increased to 5-7%.

Inorganic phosphate plays a vital role and is essential in the biological mineralization, which is throughout life and is mainly mediated by the function of osteoblasts [66-68]. The high phosphate containing BGs resulted in the phosphate concentrations in BG-conditioned medium kept similar to that in α-MEM, avoiding consuming medium phosphate to form apatite. In BG, silicon acts as network former. However, it has stimulatory effects on cellular activities, such as regulating the expression of key osteoblastic marker genes, stimulating new bone formation in animal models and inhibiting osteoclast phenotypic gene expressions *in vitro* although the exact mechanism is yet to be understood [69-75]. In this study, the released silicon concentrations into cell culture medium were ranged from 45 to 52 ppm depending on BG composition, and may contribute to the promoted proliferation, ALP activity, collagen and bone nodule formation and osteogenic gene expression in MC3T3-E1 cells by the high phosphate but fluoride free BG (P6.33F0), compared with the control (no BG). However, these osteogenic responses were further increased in BG P6.33F1, but suppressed when the BG fluoride content increased to 5-7%. It can attribute to that fluoride interacts with mineralized tissues in a biphasic manner [19, 76] and also depends on the concentration, time and cell type (primary cells or established cell line) [77]. In this study, the glass P6.33F1 conditioned media, with a released F^- concentration around 0.15mM, significantly promoted the osteogenic responses of MC3T3-E1 cells.

For the pro-angiogenic effects, we found the VEGF gene expression and its protein production were both significantly promoted by the high phosphate, but fluoride free BG P6.33F0, and further increased in the fluoride containing BG-conditioned medium. Compared with the control, BG-conditioned medium contains silicon that was released from the BGs. Silicon, aside from the potential osteogenic benefits discussed before, has angiogenic capabilities as well [26]. Numerous *in vitro* and *in vivo* studies have demonstrated that silicon containing BGs stimulate VEGF secretion and promote angiogenesis [78-80]. In addition to BGs, utilizing a calcium silicate bioceramic resulted in VEFG expression in human dermal fibroblasts, which was mainly induced by the presence of silicon [81]. Similarly, a calcium silicate applied in a rabbit femur defect was also able to demonstrate angiogenic effects [82]. However, very few publications discussed the effects of fluoride on angiogenesis. Through embedding different sponges into rabbit femur, Lalk *et al.* found that MgF_2 coating sponges exhibited the highest vascularization [83]. The deposition of VEGF in the thyroid gland was significantly promoted through NaF water feeding in a rat model [84]. In this study, there may be combined effects of silicon and fluoride responsible for the improved angiogenic potential from MC3T3-E1 cells. A sufficient supply of blood and oxygen is a key and dependent factor for osteogenesis in bone healing [85-87]. The fluoride containing glasses exhibit angiogenic potential *in vitro* and could be used as bone substitutes with the expected promotion of VEGF gene expression and protein production *in vitro*.

Periodontal disease is a bacterially induced inflammatory disease resulting in the destruction of soft and hard tooth-supporting (periodontal) tissues [88]. Peri-implantitis is also an inflammatory reaction associated with supporting bone loss around the dental implants and mainly caused by periodontal pathogens. *P. gingivalis* is highly associated with the chronic periodontitis, and can be detected in up to 85% of the disease sites [89]. *A. actinomycetemcomitans* is mainly detected in aggressive periodontitis, a severe and rapidly progressing form which most often starts at an early age [90]. In this study, the growth of both bacteria was significantly inhibited after incubation with the bioactive glass particulates. Bacteria were also sensitive in a dose dependent manner to the NaF concentrations. Numerous studies have demonstrated that the antimicrobial activity of fluoride, such as, in a 30min exposure test, both bacterial strains, *A. actinomycetemcomitans* and *P. gingivalis*,

exhibited a significant decrease of colony-forming units in a NaF concentration-dependent manner [91]. A 6-month clinical study found that the fluoride containing dentifrice showed significant reductions in the number of anaerobic bacteria on both the dental implants and control teeth at 3 months [92]. Further, fluoride surface-modified titanium specimens significantly inhibited the growth of both *P. gingivalis* and *A. actinomycetemcomitans* than the polished titanium [93].

However, even the base glass P6.33F0 in this study showed some degree of antibacterial activity, especially against *P. gingivalis*. Several studies have demonstrated that BG, without specific ionic additions, has a clear growth-inhibitory effect against numerous clinically important pathogens such as *S. aureus*, *E. coli*, *F. necrophorum*, *P. gingivalis*, *S. mutans*, *A.actinomycetemcomitans* [94-97]. The antibacterial mechanism of BG is based on the pH elevation, unfavorable for bacteria, caused by the BG sodium release and increased osmotic pressure from ions (silicon, calcium, sodium and phosphate) dissolution, creating an environment where the bacteria cannot grow [98]. The incorporation of specific antibacterial ion F into BGs in this study significantly promoted the antimicrobial activity against periodontal pathogens.

Conclusion

In summary, we have shown that the low F^-/high P_2O_5 BGs resulted in significantly faster apatite formation in Tris buffer solution, and promoted osteoblast-like cell pre-osteogenic, pro-angiogenic responses and significantly inhibited the growth of two important periodontal pathogens *in vitro*. Such novel low F^-/high P_2O_5 BGs would be expected to stimulate bone formation and overcome problems associated with infection and the poor vascularisation in large bone graft sites and reduce the need for further clinical intervention.

Acknowledgments

Jie Liu was supported by China Scholarship Council (CSC)/Queen Mary University of London Joint PhD scholarships

Author Contributions

All the co-authors of the paper have contributed to the research and writing of the paper. Jie Liu performed the studies. Robert Hill contributed to the BGs study. Simon

Rawlinson contributed to the design of the biological experiments. Farida Fortune directed the research.

Conflicts of Interest

The authors declare no conflict of interest.

References:

[1] Hench LL. The story of Bioglass. J Mater Sci Mater Med. 2006;17:967-78.
[2] Hench LL, Splinter RJ, Allen WC, Greenlee TK. Bonding mechanisms at the interface of ceramic prosthetic materials. Journal of Biomedical Materials Research. 1971;5:117-41.
[3] O'Donnell MD, Watts SJ, Hill RG, Law RV. The effect of phosphate content on the bioactivity of soda-lime-phosphosilicate glasses. J Mater Sci Mater Med. 2009;20:1611-8.
[4] O'Donnell MD, Watts SJ, Law RV, Hill RG. Effect of P2O5 content in two series of soda lime phosphosilicate glasses on structure and properties – Part I: NMR. Journal of Non-Crystalline Solids. 2008;354:3554-60.
[5] O'Donnell MD, Watts SJ, Law RV, Hill RG. Effect of P2O5 content in two series of soda lime phosphosilicate glasses on structure and properties – Part II: Physical properties. Journal of Non-Crystalline Solids. 2008;354:3561-6.
[6] Edén M. The split network analysis for exploring composition–structure correlations in multi-component glasses: I. Rationalizing bioactivity-composition trends of bioglasses. Journal of Non-Crystalline Solids. 2011;357:1595-602.
[7] Brauer DS, Karpukhina N, Law RV, Hill RG. Structure of fluoride-containing bioactive glasses. Journal of Materials Chemistry. 2009;19:5629-36.
[8] Brauer DS, Karpukhina N, O'Donnell MD, Law RV, Hill RG. Fluoride-containing bioactive glasses: Effect of glass design and structure on degradation, pH and apatite formation in simulated body fluid. Acta Biomaterialia. 2010;6:3275-82.
[9] Delia S. Brauer NK, Daphne Seah, Robert V. Law, Robert G. Hill. Fluoride-Containing Bioactive Glasses. Advanced Materials Research. 2008;(Volumes 39 - 40:299-304.
[10] Al-Noaman A, Karpukhina N, Rawlinson SCF, Hill RG. Effect of FA on bioactivity of bioactive glass coating for titanium dental implant. Part I: Composite powder. Journal of Non-Crystalline Solids. 2013;364:92-8.
[11] Farley JR, Wergedal JE, Baylink DJ. Fluoride directly stimulates proliferation and alkaline phosphatase activity of bone-forming cells. Science (New York, NY). 1983;222:330-2.
[12] Huo L, Liu K, Pei J, Yang Y, Ye Y, Liu Y, et al. Flouride Promotes Viability and Differentiation of Osteoblast-Like Saos-2 Cells Via BMP/Smads Signaling Pathway. Biol Trace Elem Res. 2013.
[13] Pei J, Li B, Gao Y, Wei Y, Zhou L, Yao H, et al. Fluoride decreased osteoclastic bone resorption through the inhibition of NFATc1 gene expression. Environ Toxicol. 2012.
[14] Qu WJ, Zhong DB, Wu PF, Wang JF, Han B. Sodium fluoride modulates caprine osteoblast proliferation and differentiation. J Bone Miner Metab. 2008;26:328-34.
[15] Ren G, Wang K, Chang R, Su Y, Wang J, Su J, et al. Simultaneous administration of fluoride and selenite regulates proliferation and apoptosis in murine osteoblast-like MC3T3-E1 cells by altering osteoprotegerin. Biol Trace Elem Res. 2011;144:1437-48.

[16] Wang Z, Yang X, Yang S, Ren G, Ferreri M, Su Y, et al. Sodium fluoride suppress proliferation and induce apoptosis through decreased insulin-like growth factor-I expression and oxidative stress in primary cultured mouse osteoblasts. Arch Toxicol. 2011;85:1407-17.
[17] Yan X, Feng C, Chen Q, Li W, Wang H, Lv L, et al. Effects of sodium fluoride treatment in vitro on cell proliferation, apoptosis and caspase-3 and caspase-9 mRNA expression by neonatal rat osteoblasts. Arch Toxicol. 2009;83:451-8.
[18] von Tirpitz C, Klaus J, Steinkamp M, Hofbauer LC, Kratzer W, Mason R, et al. Therapy of osteoporosis in patients with Crohn's disease: a randomized study comparing sodium fluoride and ibandronate. Alimentary pharmacology & therapeutics. 2003;17:807-16.
[19] Chachra D, Vieira AP, Grynpas MD. Fluoride and mineralized tissues. Crit Rev Biomed Eng. 2008;36:183-223.
[20] Vestergaard P, Jorgensen NR, Schwarz P, Mosekilde L. Effects of treatment with fluoride on bone mineral density and fracture risk--a meta-analysis. Osteoporos Int. 2008;19:257-68.
[21] Collin-Osdoby P. Role of vascular endothelial cells in bone biology. J Cell Biochem. 1994;55:304-9.
[22] Ferrara N. Vascular endothelial growth factor: basic science and clinical progress. Endocrine reviews. 2004;25:581-611.
[23] Weibing Z, Wang L. [Correlation between vascular endothelial growth factor temporal expression and new bone formation in midpalatal suture during rapid maxillary expansion]. Hua xi kou qiang yi xue za zhi = Huaxi kouqiang yixue zazhi = West China journal of stomatology. 2014;32:561-5.
[24] Schliephake H, Rublack J, Forster A, Schwenzer B, Reichert J, Scharnweber D. Functionalization of titanium implants using a modular system for binding and release of VEGF enhances bone implant contact in a rodent model. Journal of clinical periodontology. 2015.
[25] Izuagie IA, Pelham CJ, Agrawal DK. Synergistic effect of angiotensin II on vascular endothelial growth factor-A-mediated differentiation of bone marrow-derived mesenchymal stem cells into endothelial cells. Stem cell research & therapy. 2015;6:4.
[26] Bose S, Fielding G, Tarafder S, Bandyopadhyay A. Understanding of dopant-induced osteogenesis and angiogenesis in calcium phosphate ceramics. Trends Biotechnol. 2013;31:594-605.
[27] Yuan K, Chan YJ, Kung KC, Lee TM. Comparison of osseointegration on various implant surfaces after bacterial contamination and cleaning: a rabbit study. The International journal of oral & maxillofacial implants. 2014;29:32-40.
[28] van Winkelhoff AJ, Goene RJ, Benschop C, Folmer T. Early colonization of dental implants by putative periodontal pathogens in partially edentulous patients. Clin Oral Implants Res. 2000;11:511-20.
[29] Burke FM, Ray NJ, McConnell RJ. Fluoride-containing restorative materials. International dental journal. 2006;56:33-43.
[30] Van Loveren C. Antimicrobial activity of fluoride and its in vivo importance: identification of research questions. Caries research. 2001;35 Suppl 1:65-70.
[31] Kawashima J, Nakajo K, Washio J, Mayanagi G, Shimauchi H, Takahashi N. Fluoride-sensitivity of growth and acid production of oral Actinomyces: comparison with oral Streptococcus. Microbiology and immunology. 2013;57:797-804.
[32] Marquis RE. Antimicrobial actions of fluoride for oral bacteria. Canadian journal of microbiology. 1995;41:955-64.
[33] Lellouche J, Kahana E, Elias S, Gedanken A, Banin E. Antibiofilm activity of nanosized magnesium fluoride. Biomaterials. 2009;30:5969-78.
[34] Mneimne M, Hill RG, Bushby AJ, Brauer DS. High phosphate content significantly increases apatite formation of fluoride-containing bioactive glasses. Acta Biomater. 2011;7:1827-34.
[35] Brauer DS, Mneimne M, Hill RG. Fluoride-containing bioactive glasses: Fluoride loss during melting and ion release in tris buffer solution. Journal of Non-Crystalline Solids. 2011;357:3328-33.

[36] van Meerloo J, Kaspers GJ, Cloos J. Cell sensitivity assays: the MTT assay. Methods Mol Biol. 2011;731:237-45.
[37] Rago R, Mitchen J, Wilding G. DNA fluorometric assay in 96-well tissue culture plates using Hoechst 33258 after cell lysis by freezing in distilled water. Anal Biochem. 1990;191:31-4.
[38] Effah Kaufmann EA, Ducheyne P, Shapiro IM. Evaluation of osteoblast response to porous bioactive glass (45S5) substrates by RT-PCR analysis. Tissue Eng. 2000;6:19-28.
[39] Lee JH, Ryu MY, Baek HR, Lee KM, Seo JH, Lee HK, et al. Effects of porous beta-tricalcium phosphate-based ceramics used as an E. coli-derived rhBMP-2 carrier for bone regeneration. J Mater Sci Mater Med. 2013.
[40] Ma W, Zhang X, Shi S, Zhang Y. Neuropeptides stimulate human osteoblast activity and promote gap junctional intercellular communication. Neuropeptides. 2013;47:179-86.
[41] Lim PN, Chang L, Tay BY, Guneta V, Choong C, Ho B, et al. Proposed mechanism of antibacterial action of chemically modified apatite for reduced bone infection. ACS applied materials & interfaces. 2014;6:17082-92.
[42] Junqueira LC, Bignolas G, Brentani RR. Picrosirius staining plus polarization microscopy, a specific method for collagen detection in tissue sections. The Histochemical journal. 1979;11:447-55.
[43] Kliment CR, Englert JM, Crum LP, Oury TD. A novel method for accurate collagen and biochemical assessment of pulmonary tissue utilizing one animal. International journal of clinical and experimental pathology. 2011;4:349-55.
[44] Stanford CM, Jacobson PA, Eanes ED, Lembke LA, Midura RJ. Rapidly forming apatitic mineral in an osteoblastic cell line (UMR 106-01 BSP). J Biol Chem. 1995;270:9420-8.
[45] Carpenter CD, O'Neill T, Picot N, Johnson JA, Robichaud GA, Webster D, et al. Anti-mycobacterial natural products from the Canadian medicinal plant Juniperus communis. Journal of ethnopharmacology. 2012;143:695-700.
[46] Collins L, Franzblau SG. Microplate alamar blue assay versus BACTEC 460 system for high-throughput screening of compounds against Mycobacterium tuberculosis and Mycobacterium avium. Antimicrobial agents and chemotherapy. 1997;41:1004-9.
[47] Lu X, Leng Y. Theoretical analysis of calcium phosphate precipitation in simulated body fluid. Biomaterials. 2005;26:1097-108.
[48] Jones JR, Sepulveda P, Hench LL. Dose-dependent behavior of bioactive glass dissolution. J Biomed Mater Res. 2001;58:720-6.
[49] Shah FA, Brauer DS, Wilson RM, Hill RG, Hing KA. Influence of cell culture medium composition on in vitro dissolution behavior of a fluoride-containing bioactive glass. J Biomed Mater Res A. 2014;102:647-54.
[50] Aoba T. The effect of fluoride on apatite structure and growth. Crit Rev Oral Biol Med. 1997;8:136-53.
[51] Iijima M. Formation of octacalcium phosphate in vitro. Monographs in oral science. 2001;18:17-49.
[52] Johnsson MS, Nancollas GH. The role of brushite and octacalcium phosphate in apatite formation. Crit Rev Oral Biol Med. 1992;3:61-82.
[53] LeGeros RZ, Daculsi G, Orly I, Abergas T, Torres W. Solution-mediated transformation of octacalcium phosphate (OCP) to apatite. Scanning microscopy. 1989;3:129-37; discussion 37-8.
[54] Siew C, Gruninger SE, Chow LC, Brown WE. Procedure for the study of acidic calcium phosphate precursor phases in enamel mineral formation. Calcif Tissue Int. 1992;50:144-8.
[55] Tseng YH, Mou CY, Chan JC. Solid-state NMR study of the transformation of octacalcium phosphate to hydroxyapatite: a mechanistic model for central dark line formation. J Am Chem Soc. 2006;128:6909-18.
[56] Eanes ED, Meyer JL. The influence of fluoride on apatite formation from unstable supersaturated solutions at pH 7.4. J Dent Res. 1978;57:617-24.
[57] Iijima M, Moradian-Oldak J. Control of apatite crystal growth in a fluoride containing amelogenin-rich matrix. Biomaterials. 2005;26:1595-603.

[58] Fan Y, Sun Z, Moradian-Oldak J. Effect of fluoride on the morphology of calcium phosphate crystals grown on acid-etched human enamel. Caries research. 2009;43:132-6.
[59] Fan Y, Sun Z, Wang R, Abbott C, Moradian-Oldak J. Enamel inspired nanocomposite fabrication through amelogenin supramolecular assembly. Biomaterials. 2007;28:3034-42.
[60] Sepulveda P, Jones JR, Hench LL. In vitro dissolution of melt-derived 45S5 and sol-gel derived 58S bioactive glasses. J Biomed Mater Res. 2002;61:301-11.
[61] Diba M, Tapia F, Boccaccini AR, Strobel LA. Magnesium-Containing Bioactive Glasses for Biomedical Applications. International Journal of Applied Glass Science. 2012;3:221-53.
[62] Barrere F, van BC, de GK, Layrolle P. Nucleation of biomimetic Ca-P coatings on ti6A14V from a SBF x 5 solution: influence of magnesium. Biomaterials. 2002;23:2211-20.
[63] Dietrich E, Oudadesse H, Lucas-Girot A, Mami M. In vitro bioactivity of melt-derived glass 46S6 doped with magnesium. J Biomed Mater Res A. 2009;88:1087-96.
[64] Ma J, Chen CZ, Wang DG, Hu JH. Effect of magnesia on structure, degradability and in vitro bioactivity of CaO–MgO–P2O5–SiO2 system ceramics. Materials Letters. 2011;65:130-3.
[65] Vallet-Regi M, J. Salinas A, Roman J, Gil M. Effect of magnesium content on the in vitro bioactivity of CaO-MgO-SiO2-P2O5 sol-gel glasses. Journal of Materials Chemistry. 1999;9:515-8.
[66] Beck GR, Jr. Inorganic phosphate as a signaling molecule in osteoblast differentiation. J Cell Biochem. 2003;90:234-43.
[67] Beck GR, Jr., Moran E, Knecht N. Inorganic phosphate regulates multiple genes during osteoblast differentiation, including Nrf2. Exp Cell Res. 2003;288:288-300.
[68] Beck GR, Jr., Sullivan EC, Moran E, Zerler B. Relationship between alkaline phosphatase levels, osteopontin expression, and mineralization in differentiating MC3T3-E1 osteoblasts. J Cell Biochem. 1998;68:269-80.
[69] Calvo-Guirado JL, Garces M, Delgado-Ruiz RA, Ramirez Fernandez MP, Ferres-Amat E, Romanos GE. Biphasic beta-TCP mixed with silicon increases bone formation in critical site defects in rabbit calvaria. Clin Oral Implants Res. 2014.
[70] Chadwick EG, Clarkin OM, Raghavendra R, Tanner DA. A bioactive metallurgical grade porous silicon-polytetrafluoroethylene sheet for guided bone regeneration applications. Bio-medical materials and engineering. 2014;24:1563-74.
[71] Friederichs RJ, Brooks RA, Ueda M, Best SM. In vitro osteoclast formation and resorption of silicon-substituted hydroxyapatite ceramics. J Biomed Mater Res A. 2015.
[72] Henstock JR, Canham LT, Anderson SI. Silicon: the evolution of its use in biomaterials. Acta Biomater. 2015;11:17-26.
[73] Manchon A, Alkhraisat M, Rueda-Rodriguez C, Torres J, Prados-Frutos JC, Ewald A, et al. Silicon calcium phosphate ceramic as novel biomaterial to simulate the bone regenerative properties of autologous bone. J Biomed Mater Res A. 2015;103:479-88.
[74] Mladenovic Z, Johansson A, Willman B, Shahabi K, Bjorn E, Ransjo M. Soluble silica inhibits osteoclast formation and bone resorption in vitro. Acta Biomater. 2014;10:406-18.
[75] Odatsu T, Azimaie T, Velten MF, Vu M, Lyles MB, Kim HK, et al. Human periosteum cell osteogenic differentiation enhanced by ionic silicon release from porous amorphous silica fibrous scaffolds. J Biomed Mater Res A. 2015.
[76] Aaseth J, Shimshi M, Gabrilove JL, Birketvedt GS. Fluoride: A toxic or therapeutic agent in the treatment of osteoporosis? The Journal of Trace Elements in Experimental Medicine. 2004;17:83-92.
[77] Everett ET. Fluoride's effects on the formation of teeth and bones, and the influence of genetics. J Dent Res. 2011;90:552-60.
[78] Day RM. Bioactive glass stimulates the secretion of angiogenic growth factors and angiogenesis in vitro. Tissue Eng. 2005;11:768-77.
[79] Gorustovich AA, Roether JA, Boccaccini AR. Effect of bioactive glasses on angiogenesis: a review of in vitro and in vivo evidences. Tissue Eng Part B Rev. 2010;16:199-207.
[80] Leu A, Stieger SM, Dayton P, Ferrara KW, Leach JK. Angiogenic response to bioactive glass promotes bone healing in an irradiated calvarial defect. Tissue Eng Part A. 2009;15:877-85.

[81] Li H, Chang J. Bioactive silicate materials stimulate angiogenesis in fibroblast and endothelial cell co-culture system through paracrine effect. Acta Biomater. 2013;9:6981-91.
[82] Wang C, Lin K, Chang J, Sun J. Osteogenesis and angiogenesis induced by porous beta-CaSiO(3)/PDLGA composite scaffold via activation of AMPK/ERK1/2 and PI3K/Akt pathways. Biomaterials. 2013;34:64-77.
[83] Lalk M, Reifenrath J, Angrisani N, Bondarenko A, Seitz JM, Mueller PP, et al. Fluoride and calcium-phosphate coated sponges of the magnesium alloy AX30 as bone grafts: a comparative study in rabbits. J Mater Sci Mater Med. 2013;24:417-36.
[84] Liu G, Zhang W, Jiang P, Li X, Liu C, Chai C. Role of nitric oxide and vascular endothelial growth factor in fluoride-induced goitrogenesis in rats. Environmental toxicology and pharmacology. 2012;34:209-17.
[85] Nuss KM, von Rechenberg B. Biocompatibility issues with modern implants in bone - a review for clinical orthopedics. The open orthopaedics journal. 2008;2:66-78.
[86] Karageorgiou V, Kaplan D. Porosity of 3D biomaterial scaffolds and osteogenesis. Biomaterials. 2005;26:5474-91.
[87] Kuzyk PR, Schemitsch EH. The basic science of peri-implant bone healing. Indian journal of orthopaedics. 2011;45:108-15.
[88] Bostanci N, Belibasakis GN. Porphyromonas gingivalis: an invasive and evasive opportunistic oral pathogen. FEMS microbiology letters. 2012;333:1-9.
[89] Tribble GD, Kerr JE, Wang BY. Genetic diversity in the oral pathogen Porphyromonas gingivalis: molecular mechanisms and biological consequences. Future microbiology. 2013;8:607-20.
[90] Brigido JA, da Silveira VR, Rego RO, Nogueira NA. Serotypes of Aggregatibacter actinomycetemcomitans in relation to periodontal status and geographic origin of individuals-a review of the literature. Medicina oral, patologia oral y cirugia bucal. 2014;19:e184-91.
[91] Shimogishi M, Tsutsumi Y, Kuroda S, Munakata M, Hanawa T, Kasugai S. Effects of acidic sodium fluoride-treated, commercially pure titanium on periodontal pathogens and rat bone marrow cells. Dent Mater J. 2014;33:70-8.
[92] Sreenivasan PK, Vered Y, Zini A, Mann J, Kolog H, Steinberg D, et al. A 6-month study of the effects of 0.3% triclosan/copolymer dentifrice on dental implants. Journal of clinical periodontology. 2011;38:33-42.
[93] Yoshinari M, Oda Y, Kato T, Okuda K. Influence of surface modifications to titanium on antibacterial activity in vitro. Biomaterials. 2001;22:2043-8.
[94] Coraca-Huber DC, Fille M, Hausdorfer J, Putzer D, Nogler M. Efficacy of antibacterial bioactive glass S53P4 against S. aureus biofilms grown on titanium discs in vitro. Journal of orthopaedic research : official publication of the Orthopaedic Research Society. 2014;32:175-7.
[95] Gergely I, Zazgyva A, Man A, Zuh SG, Pop TS. The in vitro antibacterial effect of S53P4 bioactive glass and gentamicin impregnated polymethylmethacrylate beads. Acta microbiologica et immunologica Hungarica. 2014;61:145-60.
[96] Lepparanta O, Vaahtio M, Peltola T, Zhang D, Hupa L, Hupa M, et al. Antibacterial effect of bioactive glasses on clinically important anaerobic bacteria in vitro. J Mater Sci Mater Med. 2008;19:547-51.
[97] Stoor P, Soderling E, Salonen JI. Antibacterial effects of a bioactive glass paste on oral microorganisms. Acta odontologica Scandinavica. 1998;56:161-5.
[98] Echezarreta-Lopez MM, Landin M. Using machine learning for improving knowledge on antibacterial effect of bioactive glass. International journal of pharmaceutics. 2013;453:641-7.

Tables:

Figures:

Fig. 14 Mineralised bone nodule formation. Qualitative and quantitative results of MC3T3-E1 mineralization in BG-conditioned medium. *P<0.05 or **P<0.01, compared with the control. ^{+}P<0.05, compared with P6.33F0

Fig. 15 Expression of pre-osteogenic markers. Pre-osteogenic gene expression by MC3T3-E1 of Col1a1 and OPN in BG-conditioned medium measured by qPCR. Normalized by control groups. *P<0.05 or **P<0.01, compared with the control. ^{+}P<0.05, compared with P6.33F0.

Fig. 16 VEGF gene expression. VEGF gene expression by MC3T3-E1 in BG-conditioned medium measured by qPCR. Normalized by control groups. *P<0.05 or **P<0.01, compared with control group. ^{+}P<0.05, compared with P6.33F0 group.

Fig. 17 VEGF protein production. VEGF protein production by MC3T3-E1 in BG-conditioned medium measured by Western blot. Normalized by control groups. *P<0.05 or **P<0.01, compared with control group. ^{+}P<0.05, compared with P6.33F0 group.

Fig. 18 Growth inhibition percentage of *P. gingivalis* and *A. actinomycetemcomitans* after exposure to a range of BG particle concentrations for 4 h, normalized with negative control (no glass).

Fig. 19 Growth inhibition percentage of *P. gingivalis* and *A. actinomycetemcomitans* after exposure to 1.25 mg and 10 mg BG particles, normalized with negative control (no glass).

Fig. 20 Growth inhibition percentage of *P. gingivalis* and *A. actinomycetemcomitans* after exposure to NaF concentrations, normalized with negative control (no treatment).

Fig. S1 Cell standard assay for MC3T3-E1 cells. 1500-150,000 cells, using Hoechst 33258 after lysis by brief incubation in distilled water and freezing. Insert shows a second cell standard assay for MC3T3-E1 cells, 1000-10,000 cells. Fluorescence is expressed as arbitrary units. Each marker represents mean ± S.E of eight independent experiments.

Table 1 Bioglass compositions. Compositions in mol% with increasing CaF_2 content and constant P_2O_5. NC fixed at 2.08

Glass	SiO_2	**Na_2O**	**CaO**	**P_2O_5**	**CaF_2**
P6.33F0	38.14	29.62	25.91	6.33	0
P6.33F1	37.59	29.38	25.70	6.33	1.00
P6.33F3	36.57	28.85	25.25	6.33	3.00
P6.33F5	35.55	28.33	24.79	6.33	5.00
P6.33F7	34.53	27.81	24.33	6.33	7.00

P6.33F0 named ICSW9 in previous publications [3-5]

Table 2 Sequences of primer pairs used for RT-PCR analysis

Name	**Primers 5' – 3'**
GAPDH	Forward ATTGTCAGCAATGCATCCTG
	Reverse ATGGACTGTGGTCATGAGCC
OPN	Forward GAGATTTGCTTTTGCCTGTTTG
	Reverse TGAGCTGCCAGAATCAGTCACT
Col1a1	Forward CATGTTCAGCTTTGTGGACCT
	Reverse GCAGCTGACTTCAGGGATGT
VEGF	Forward CAGGCTGCTGTAACGATGAA
	Reverse GCTTTGGTGAGGTTTGATCC

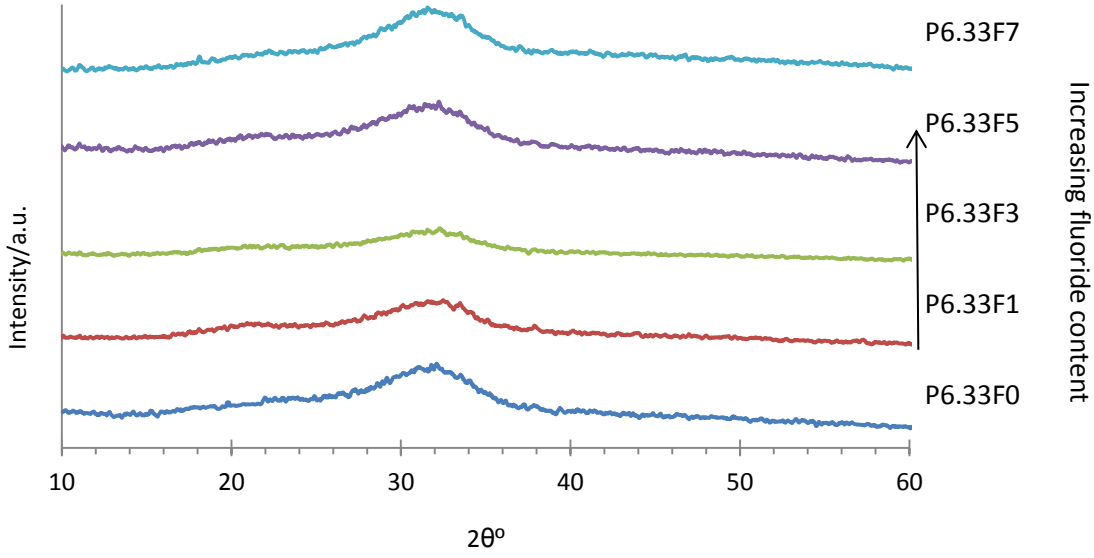
P6.33F7
P6.33F5
P6.33F3
P6.33F1
P6.33F0
Increasing fluoride content
Intensity/a.u.
10
20
30
40
50
60
2θº

Fig. 1

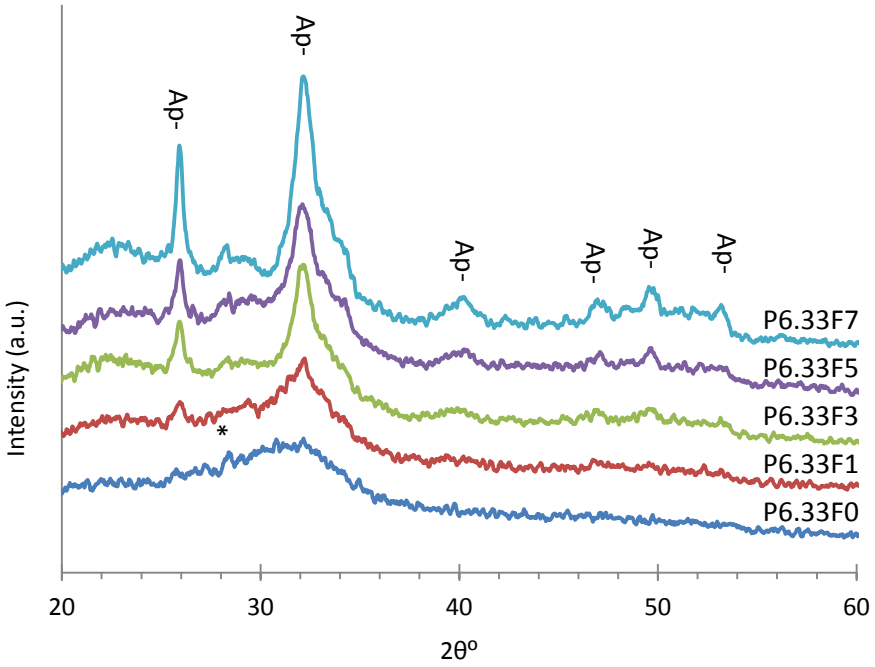
Ap-
Ap-
Ap-
Ap-
Ap-
Ap-
*
P6.33F7
P6.33F5
P6.33F3
P6.33F1
P6.33F0
Intensity (a.u.)
20
30
40
50
60
2θº

Fig. 2

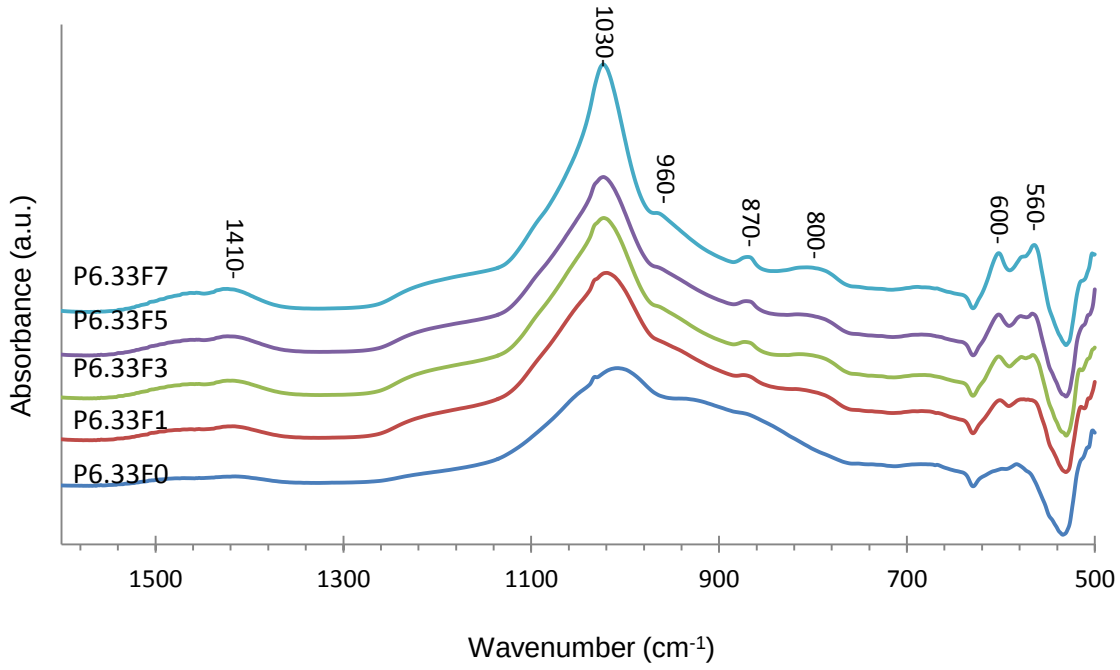
1030-
960-
870-
800-
600-
560-
1410-
P6.33F7
P6.33F5
P6.33F3
P6.33F1
P6.33F0
Absorbance (a.u.)
1500
1300
1100
900
700
500
Wavenumber (cm-1)

Fig. 3

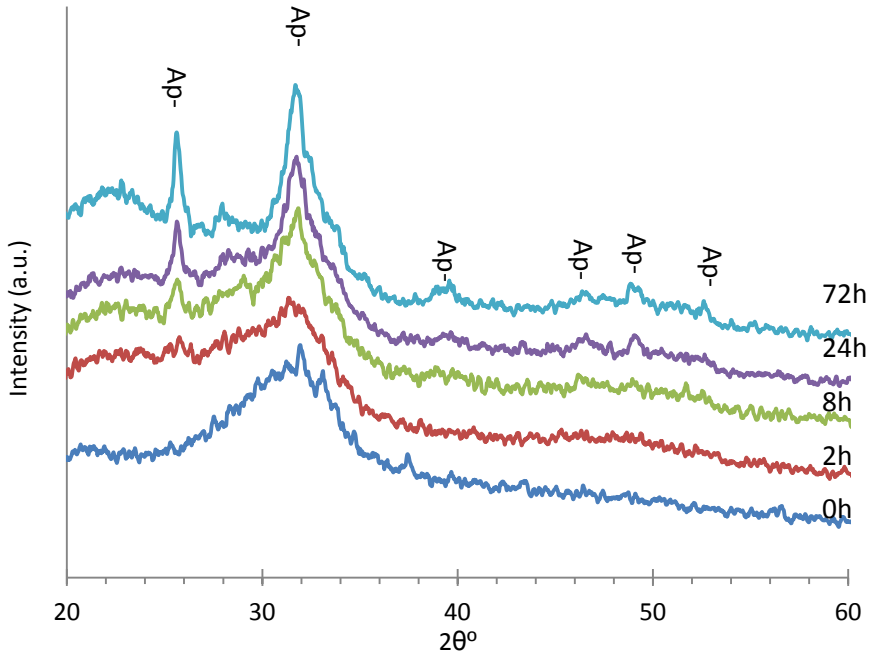
Ap-
Ap-
Ap-
Ap-
Ap-
Ap-
72h
24h
8h
2h
0h
Intensity (a.u.)
20
30
40
50
60
2θº

Fig. 4

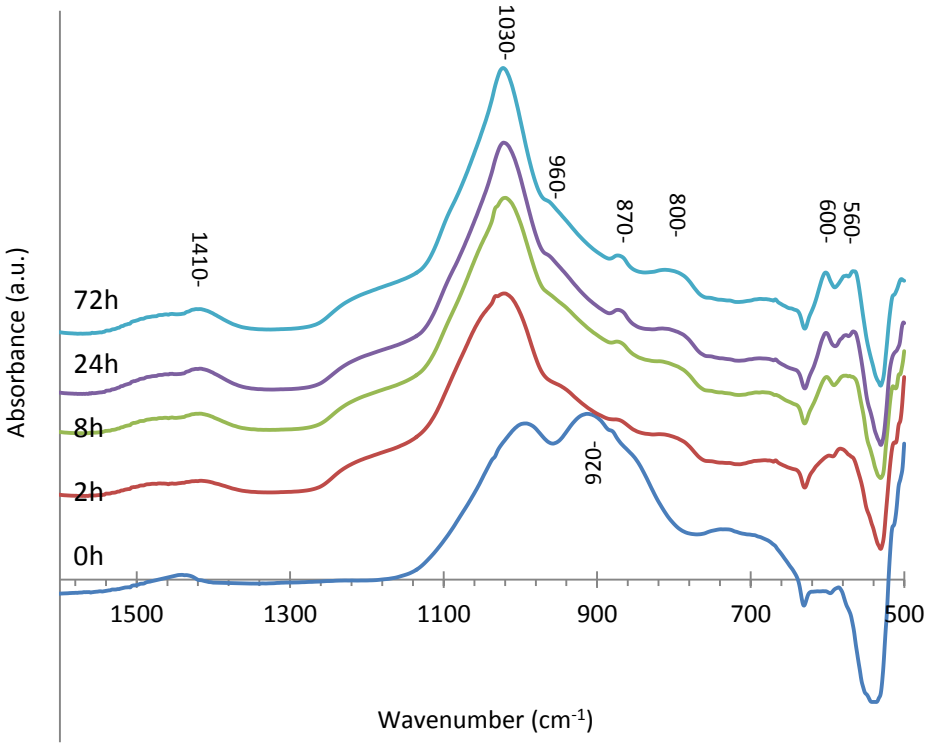
1030-
960-
870-
800-
600-
560-
1410-
920-
72h
24h
8h
2h
0h
Absorbance (a.u.)
1500
1300
1100
900
700
500
Wavenumber (cm-1)

Fig. 5

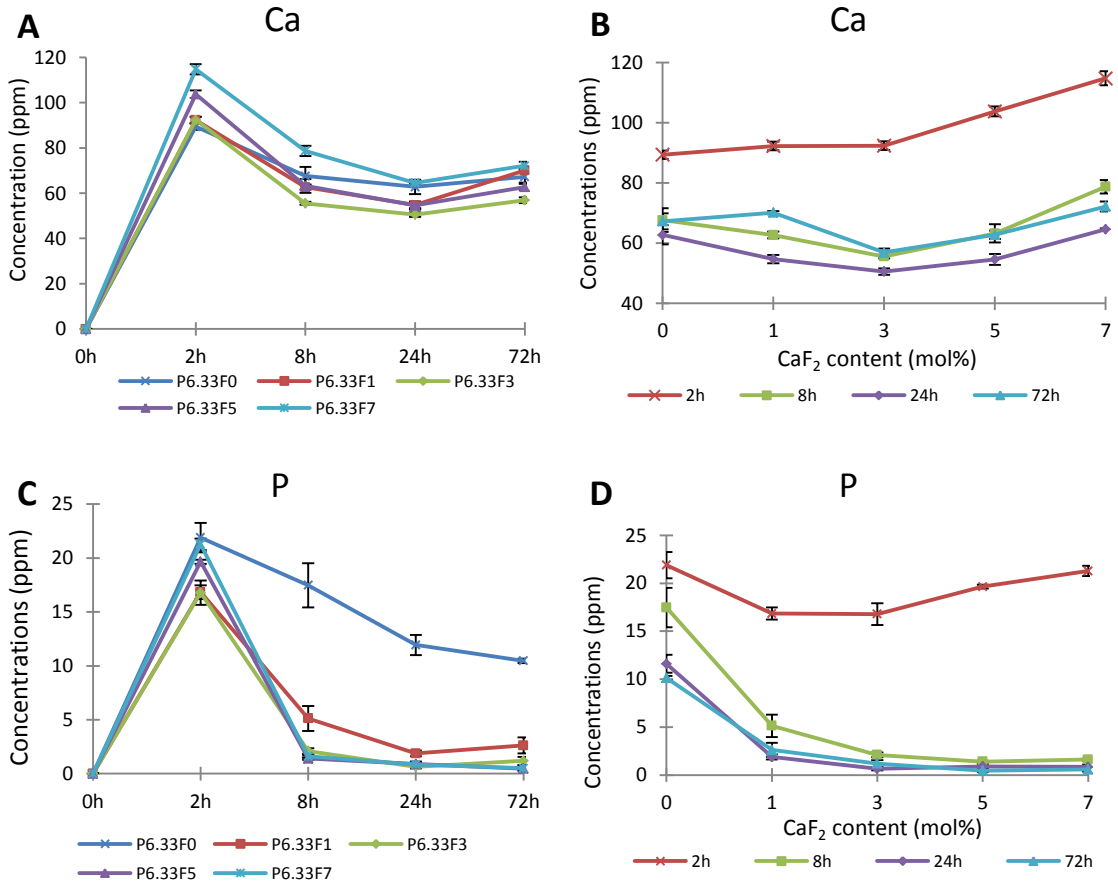
A
Ca
Concentration (ppm)
0h
2h
8h
24h
72h
P6.33F0
P6.33F1
P6.33F3
P6.33F5
P6.33F7
B
Ca
Concentrations (ppm)
CaF2 content (mol%)
2h
8h
24h
72h
C
P
Concentrations (ppm)
D
P
Concentrations (ppm)
CaF2 content (mol%)

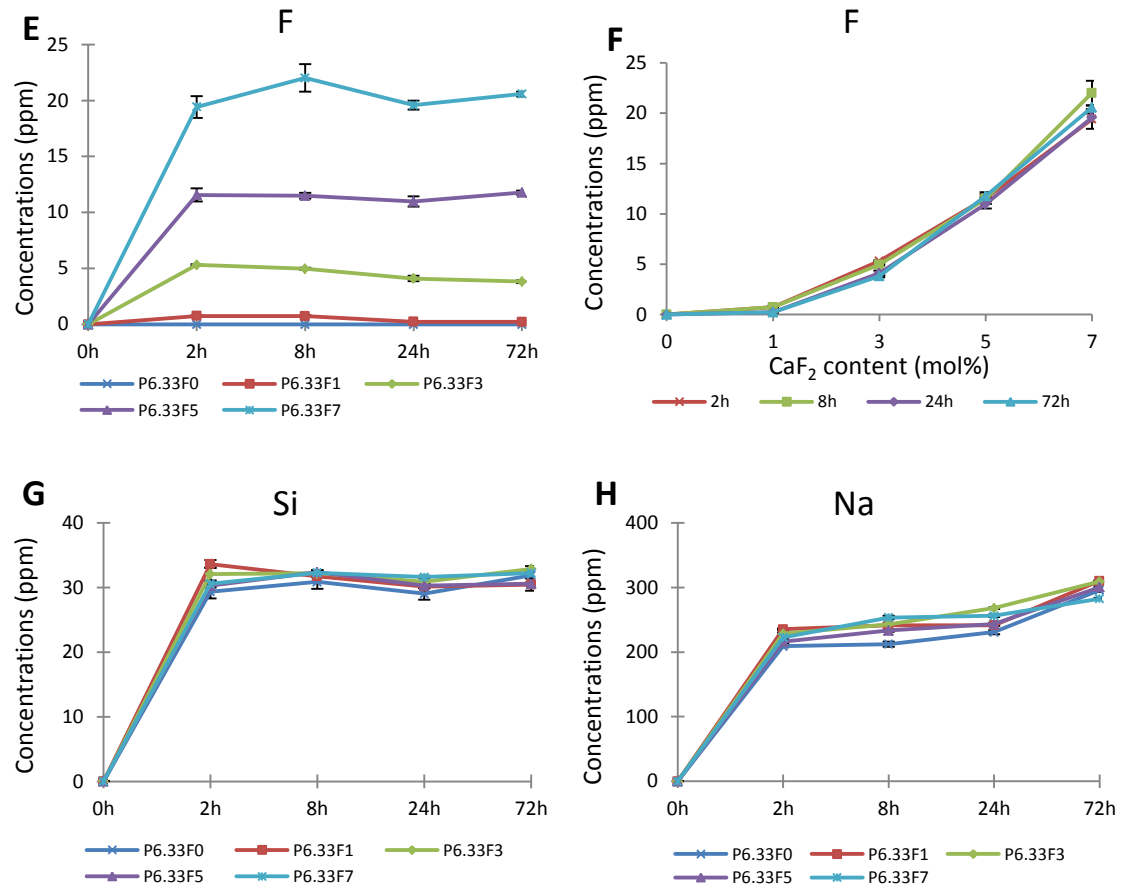
E
F
Concentrations (ppm)
0h
2h
8h
24h
72h
P6.33F0
P6.33F1
P6.33F3
P6.33F5
P6.33F7
F
Concentrations (ppm)
CaF2 content (mol%)
2h
8h
24h
72h
G
Si
Concentrations (ppm)
H
Na
Concentrations (ppm)

Fig. 6

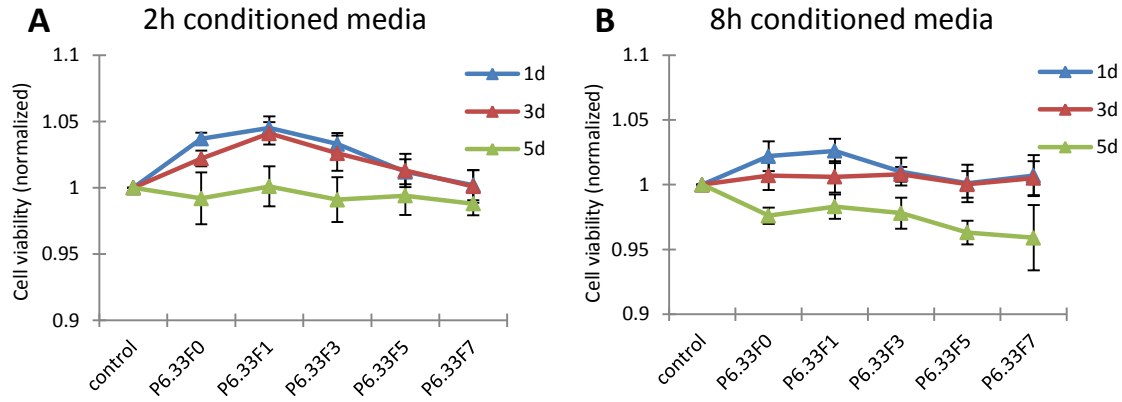
A
2h conditioned media
Cell viability (normalized)
1d
3d
5d
control
P6.33F0
P6.33F1
P6.33F3
P6.33F5
P6.33F7
B
8h conditioned media
Cell viability (normalized)

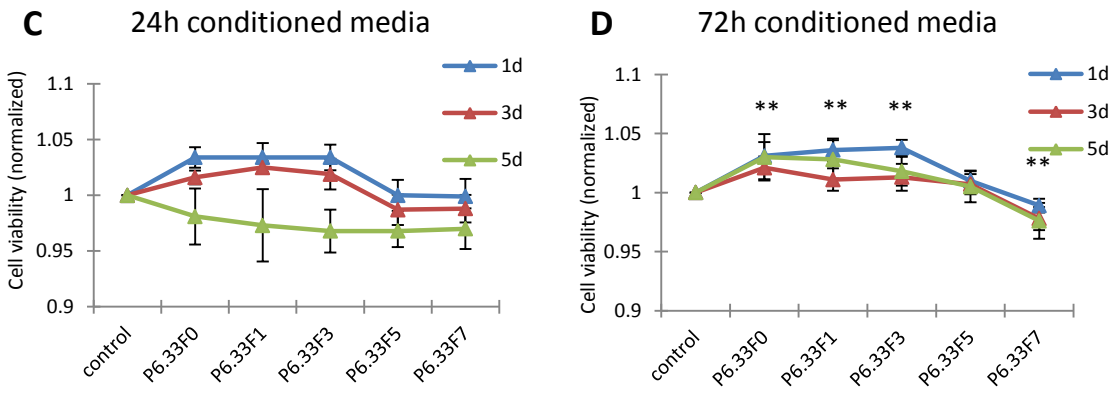
C
24h conditioned media
D
72h conditioned media
Cell viability (normalized)
1.1
1.05
1
0.95
0.9
1d
3d
5d
**
control
P6.33F0
P6.33F1
P6.33F3
P6.33F5
P6.33F7

Fig. 7

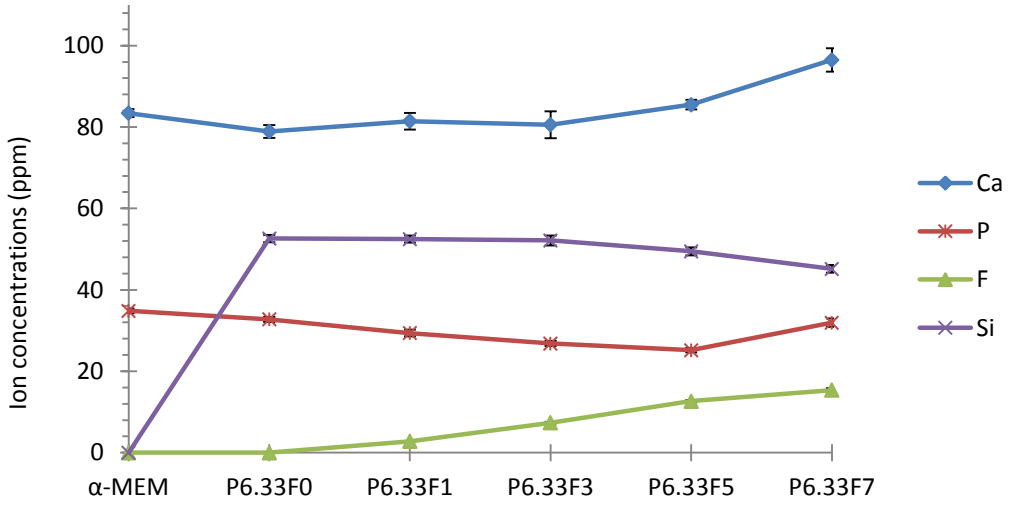
Ion concentrations (ppm)
100
80
60
40
20
0
Ca
P
F
Si
α-MEM
P6.33F0
P6.33F1
P6.33F3
P6.33F5
P6.33F7

Fig. 8

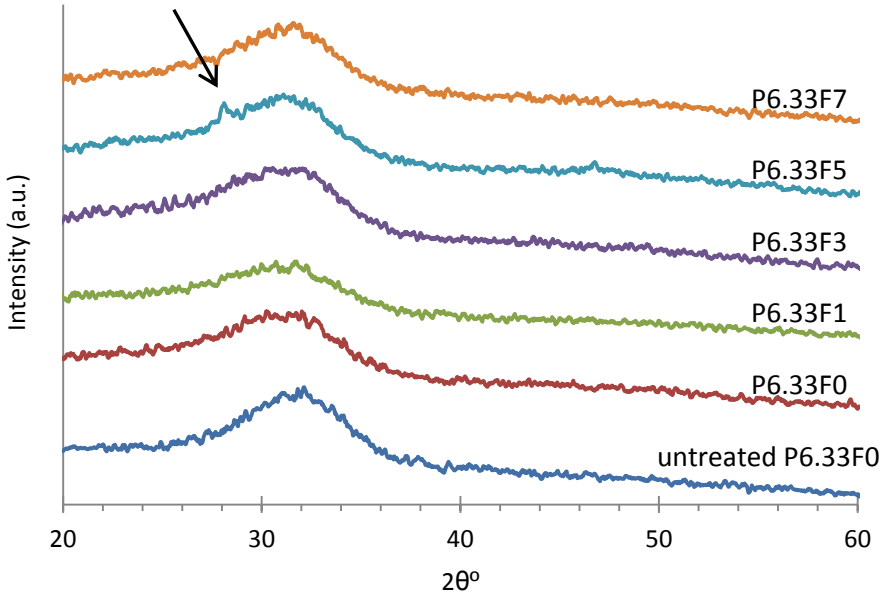
Intensity (a.u.)
P6.33F7
P6.33F5
P6.33F3
P6.33F1
P6.33F0
untreated P6.33F0
20
30
40
50
60
2θ°

Fig. 9

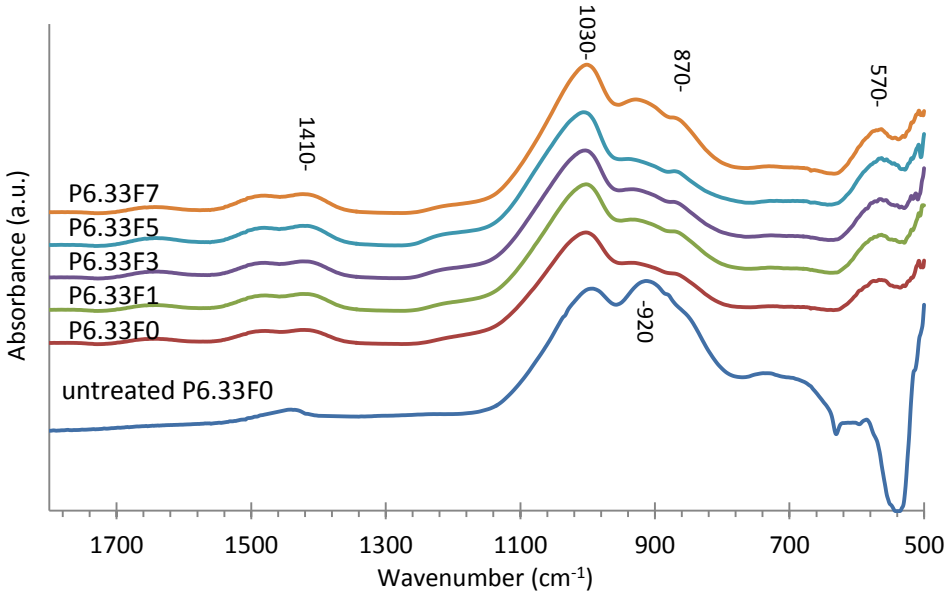

Fig. 10

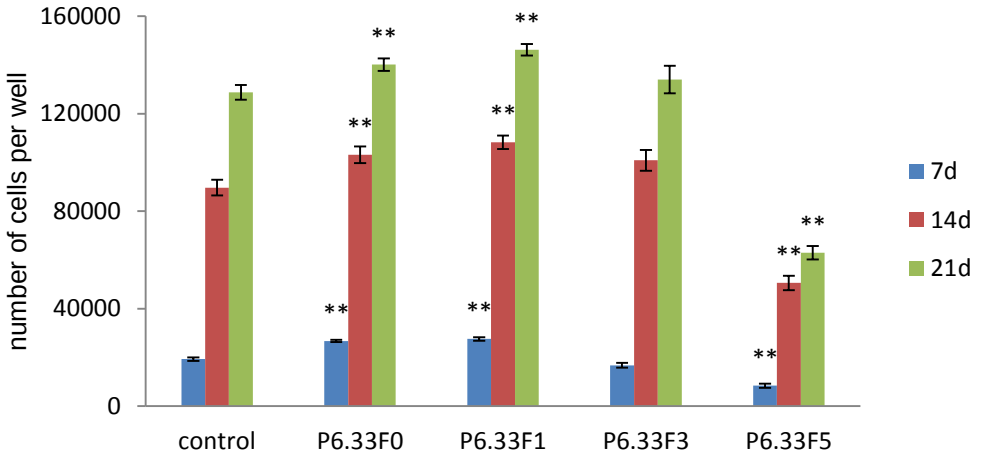

Fig. 11

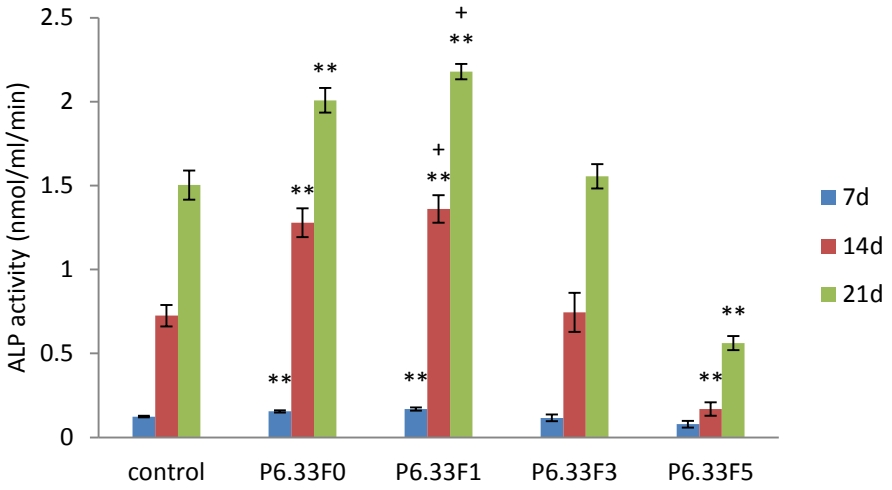
2.5
2
1.5
1
0.5
0
ALP activity (nmol/ml/min)
control
P6.33F0
P6.33F1
P6.33F3
P6.33F5
7d
14d
21d
**
+

Fig. 12

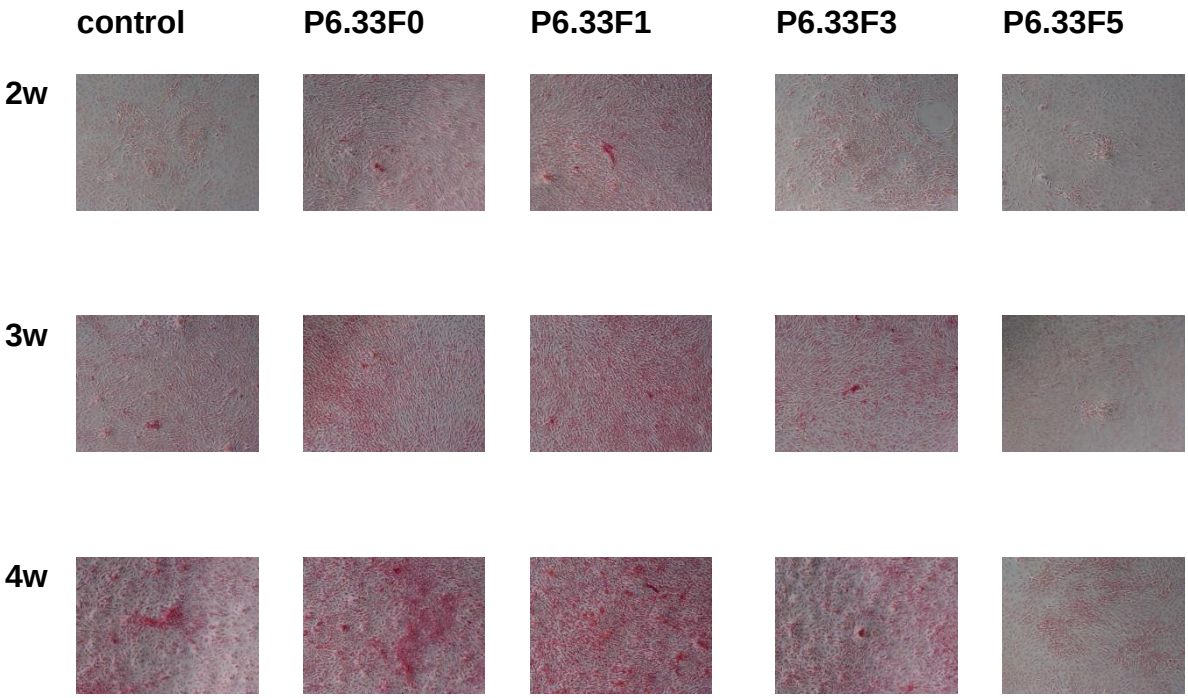
control
P6.33F0
P6.33F1
P6.33F3
P6.33F5
2w
3w
4w

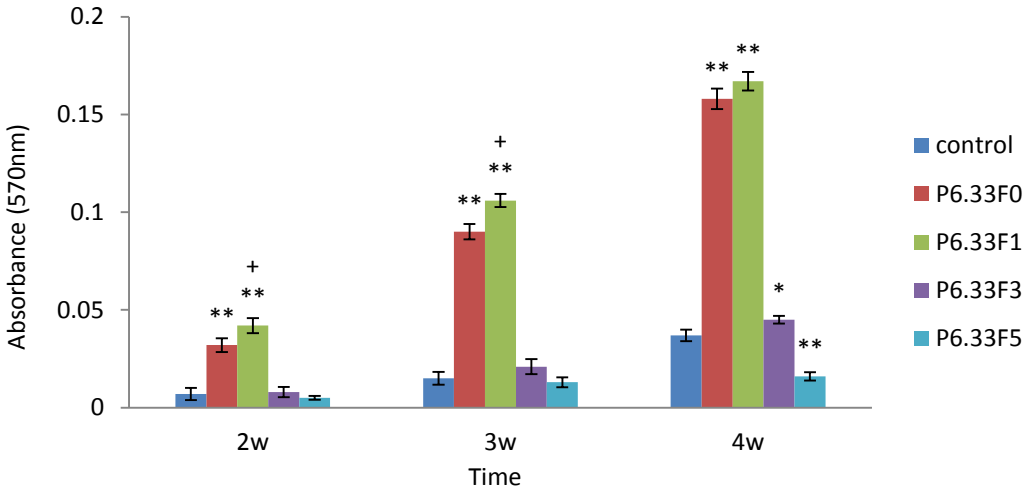
0.2
0.15
0.1
0.05
0
Absorbance (570nm)
2w
3w
4w
Time
control
P6.33F0
P6.33F1
P6.33F3
P6.33F5

Fig. 13

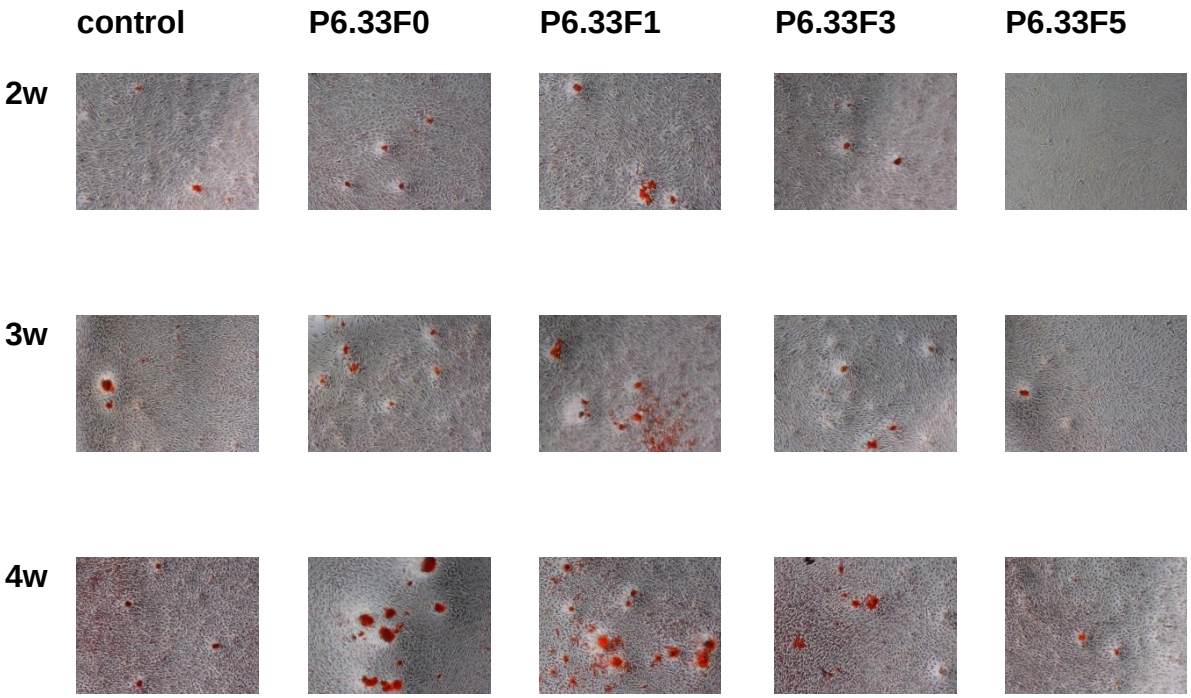
control
P6.33F0
P6.33F1
P6.33F3
P6.33F5
2w
3w
4w

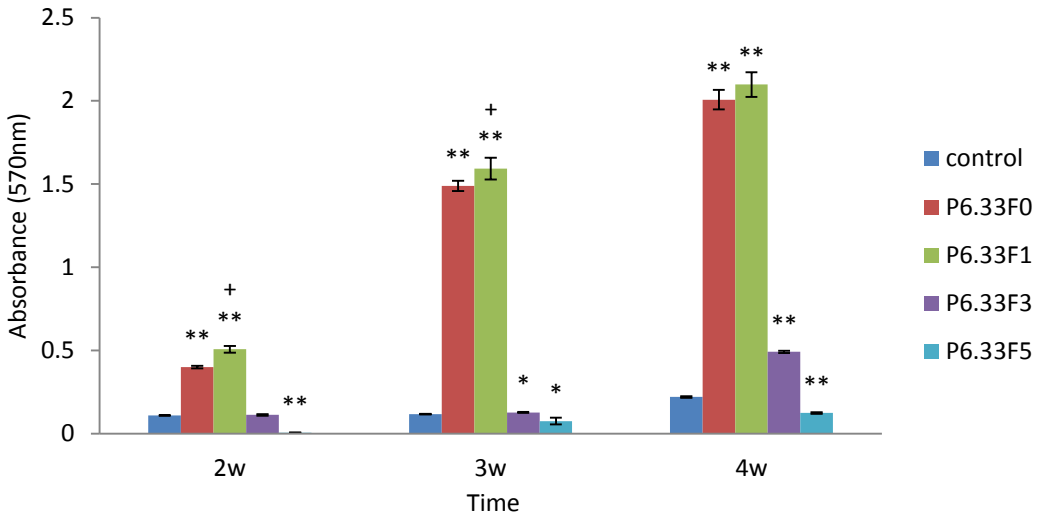
Absorbance (570nm)
2.5
2
1.5
1
0.5
0
2w
3w
4w
Time
control
P6.33F0
P6.33F1
P6.33F3
P6.33F5

Fig. 14

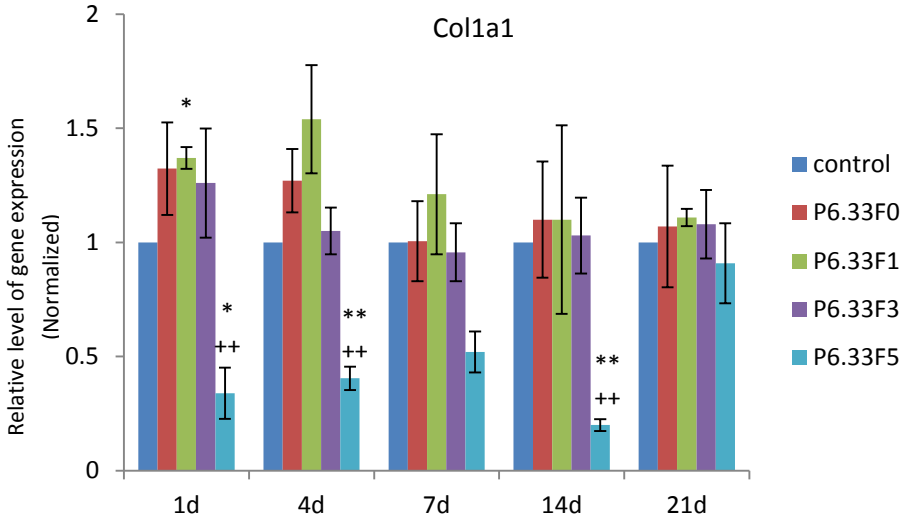
Col1a1
Relative level of gene expression (Normalized)
2
1.5
1
0.5
0
1d
4d
7d
14d
21d
control
P6.33F0
P6.33F1
P6.33F3
P6.33F5

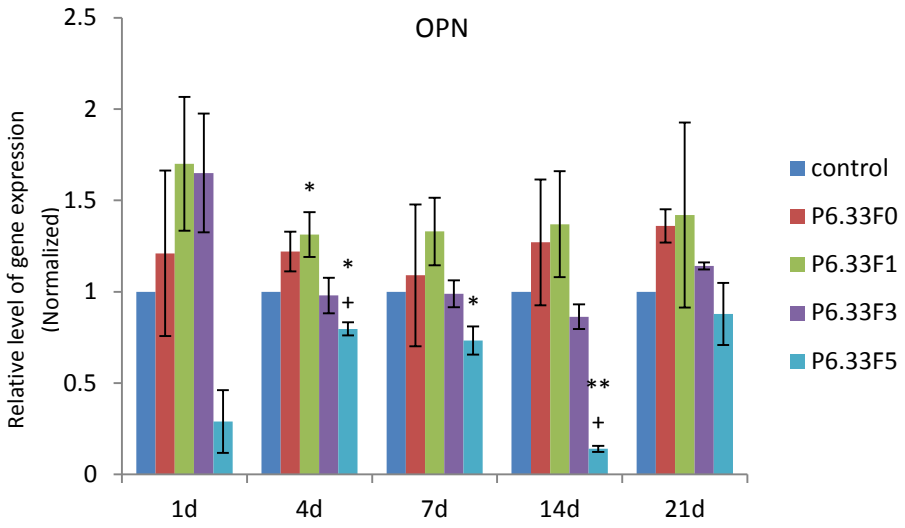
OPN
Relative level of gene expression (Normalized)
2.5
2
1.5
1
0.5
0
1d
4d
7d
14d
21d
control
P6.33F0
P6.33F1
P6.33F3
P6.33F5

Fig. 15

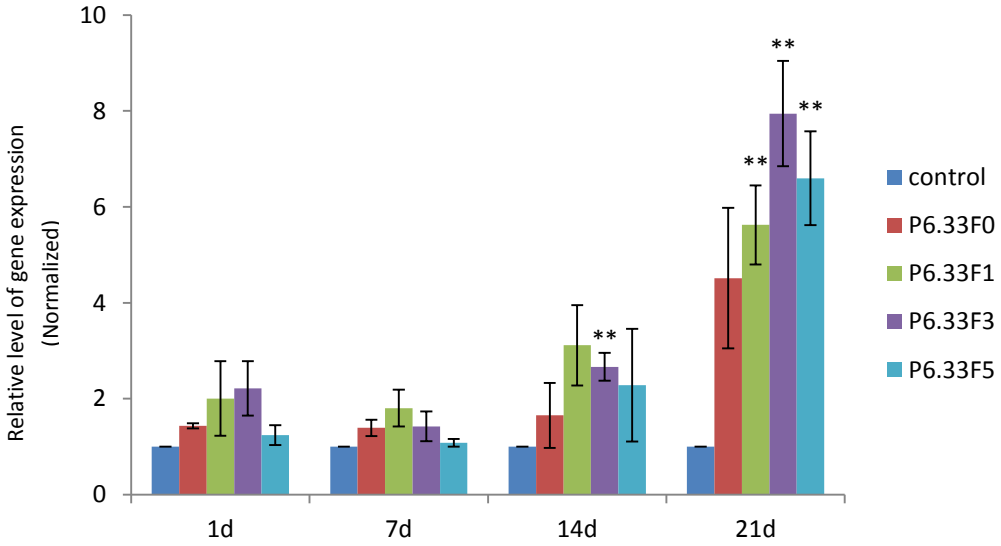
Relative level of gene expression (Normalized)
10
8
6
4
2
0
1d
7d
14d
21d
control
P6.33F0
P6.33F1
P6.33F3
P6.33F5

Fig. 16

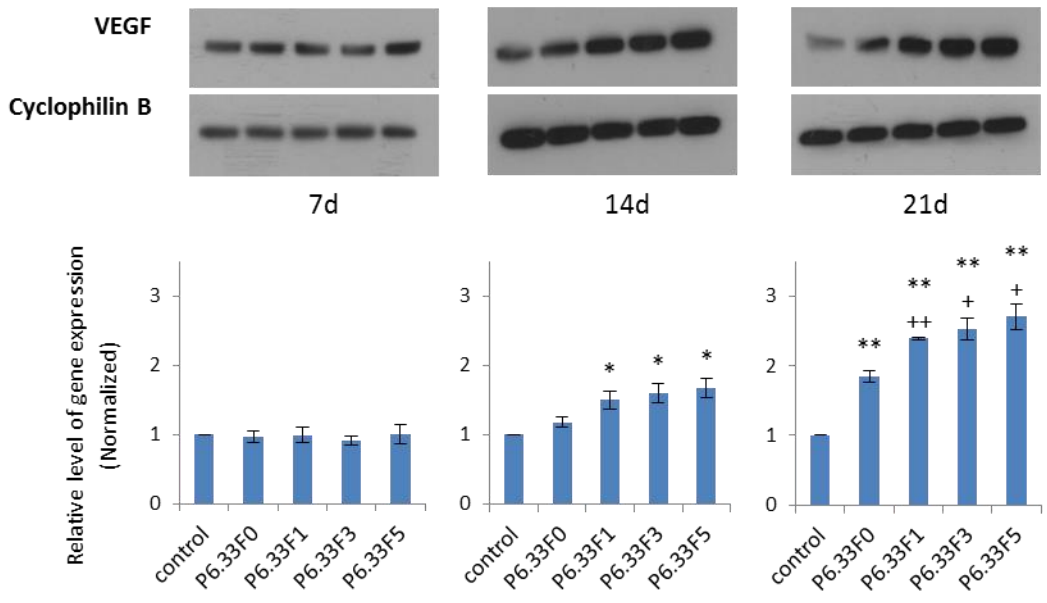
VEGF
Cyclophilin B
7d
14d
21d
Relative level of gene expression (Normalized)
control
P6.33F0
P6.33F1
P6.33F3
P6.33F5

Fig. 17

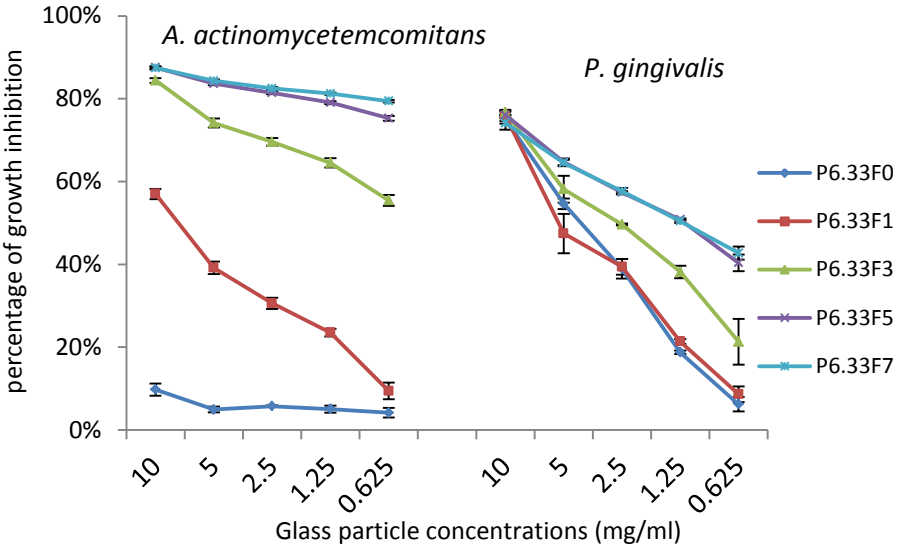
A. actinomycetemcomitans
P. gingivalis
percentage of growth inhibition
100%
80%
60%
40%
20%
0%
10
5
2.5
1.25
0.625
Glass particle concentrations (mg/ml)
P6.33F0
P6.33F1
P6.33F3
P6.33F5
P6.33F7

Fig. 18

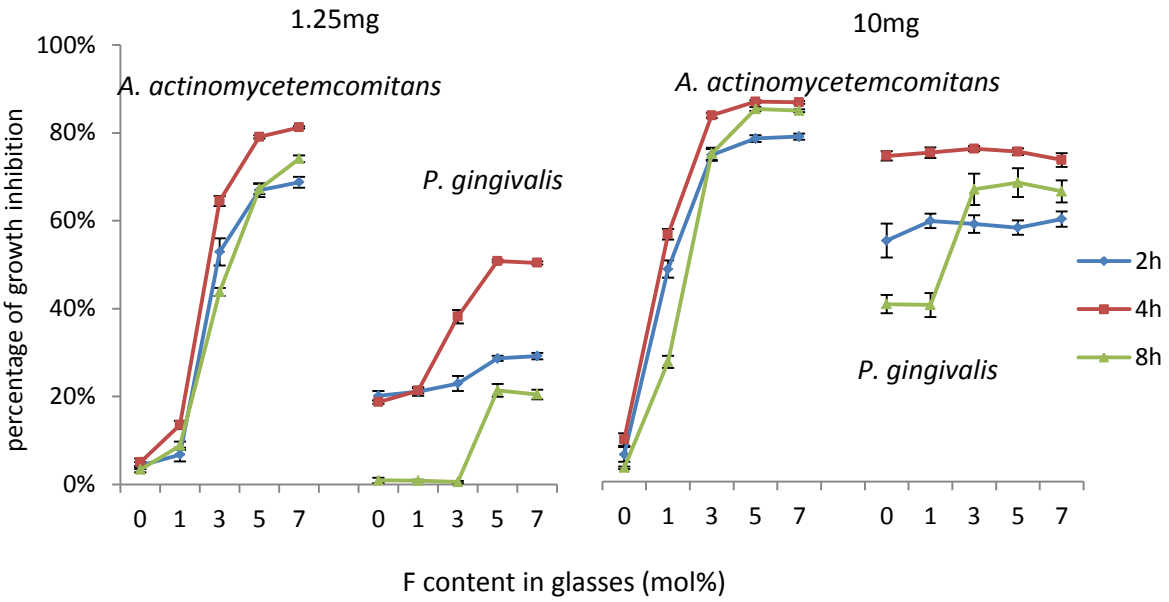
1.25mg
10mg
A. actinomycetemcomitans
P. gingivalis
A. actinomycetemcomitans
P. gingivalis
percentage of growth inhibition
100%
80%
60%
40%
20%
0%
0 1 3 5 7
0 1 3 5 7
0 1 3 5 7
0 1 3 5 7
2h
4h
8h
F content in glasses (mol%)

Fig. 19

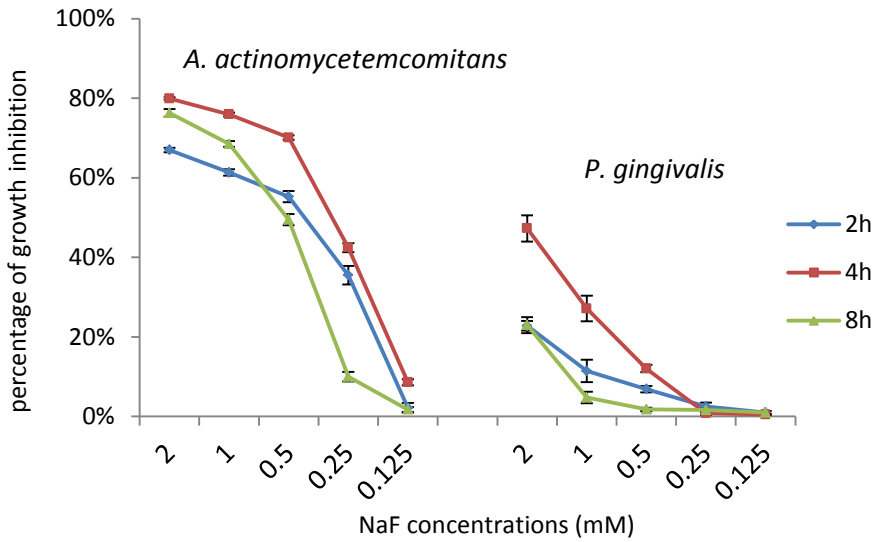
A. actinomycetemcomitans
P. gingivalis
percentage of growth inhibition
100%
80%
60%
40%
20%
0%
2 1 0.5 0.25 0.125
2 1 0.5 0.25 0.125
2h
4h
8h
NaF concentrations (mM)

Fig. 20

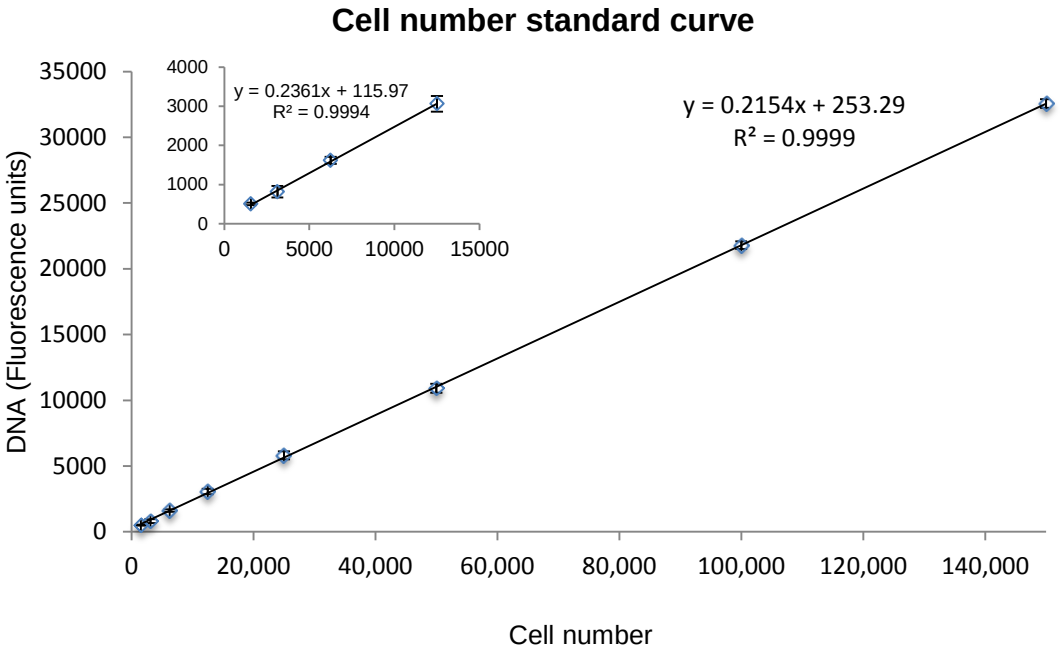
Cell number standard curve
DNA (Fluorescence units)
Cell number
y = 0.2154x + 253.29
R² = 0.9999
y = 0.2361x + 115.97
R² = 0.9994
0
5000
10000
15000
20000
25000
30000
35000
0
20,000
40,000
60,000
80,000
100,000
120,000
140,000
1000
2000
3000
4000

Fig. S1